Water Resources Research

RESEARCH ARTICLE
10.1029/2023WR035481

Constraining Plant Hydraulics With Microwave Radiometry in a Land Surface Model: Impacts of Temporal Resolution

Nataniel Holtzman[1], Yujie Wang[2], Jeffrey D. Wood[3], Christian Frankenberg[2,4], and Alexandra G. Konings[1]

[1]Department of Earth System Science, Stanford University, Stanford, CA, USA, [2]Department of Environmental Science and Engineering, California Institute of Technology, Pasadena, CA, USA, [3]School of Natural Resources, University of Missouri, Columbia, MO, USA, [4]Jet Propulsion Laboratory, California Institute of Technology, Pasadena, CA, USA

Key Points:

- We demonstrate that ecohydrological parameters and variables can be inferred from microwave radiometry via model-data fusion
- We compare scenarios that use synthetic observations at different times of day, corresponding to current and proposed satellite orbits
- For inferring land surface variables, using observations from just four times of day proves to be as useful as using data from every hour

Supporting Information:

Supporting Information may be found in the online version of this article.

Correspondence to:

N. Holtzman,
nholtzma@stanford.edu

Citation:

Holtzman, N., Wang, Y., Wood, J. D., Frankenberg, C., & Konings, A. G. (2023). Constraining plant hydraulics with microwave radiometry in a land surface model: Impacts of temporal resolution. *Water Resources Research*, *59*, e2023WR035481. https://doi.org/10.1029/2023WR035481

Received 2 JUN 2023
Accepted 4 NOV 2023

Author Contributions:

Conceptualization: Nataniel Holtzman, Jeffrey D. Wood, Christian Frankenberg, Alexandra G. Konings
Data curation: Jeffrey D. Wood
Formal analysis: Nataniel Holtzman
Funding acquisition: Jeffrey D. Wood, Christian Frankenberg, Alexandra G. Konings
Investigation: Nataniel Holtzman
Methodology: Nataniel Holtzman, Yujie Wang, Jeffrey D. Wood, Alexandra G. Konings

Abstract Vegetation water content (VWC) plays a key role in transpiration, plant mortality, and wildfire risk. Although land surface models now often contain plant hydraulics schemes, there are few direct VWC measurements to constrain these models at global scale. One proposed solution to this data gap is passive microwave remote sensing, which is sensitive to temporal changes in VWC. Here, we test that approach by using synthetic microwave observations to constrain VWC and surface soil moisture within the Climate Modeling Alliance Land model. We further investigate the possible utility of sub-daily observations of VWC, which could be obtained through a satellite in geostationary orbit or combinations of multiple satellites. These high-temporal-resolution observations could allow for improved determination of ecosystem parameters, carbon and water fluxes, and subsurface hydraulics, relative to the currently available twice-daily sun-synchronous observational patterns. We find that incorporating observations at four different times in the diurnal cycle (such as could be available from two sun-synchronous satellites) provides a significantly better constraint on water and carbon fluxes than twice-daily observations do. For example, the root mean square error of projected evapotranspiration and gross primary productivity during drought periods was reduced by approximately 40%, when using four-times-daily relative to twice-daily observations. Adding hourly observations of the entire diurnal cycle did not further improve the inferred parameters and fluxes. Our comparison of observational strategies may be informative in the design of future satellite missions to study plant hydraulics, as well as when using existing remotely sensed data to study vegetation water stress response.

Plain Language Summary The amount of water contained within the tissues of plants influences how much water plants transpire from the soil to the atmosphere and how much carbon they take in. However, it is difficult to estimate how much water is in plants around the world at any given time, due to the diversity of plants storing and releasing water in different ways. Certain earth-orbiting satellites carry sensors that can indicate plant water content, but they provide only snapshots of data at two points in time per day due to their orbit shapes. Here, we simulated what information could be gleaned from different combinations of satellites in different orbits when they are combined with computer models of water flow in plants. We found that using data from two satellites in different orbits, instead of just one, could greatly increase the accuracy of plant water content estimates, almost as much as if we had a large fleet of satellites observing around the clock. Our work should be useful to scientists studying plant water content with existing data sets as well as those planning future satellite missions.

1. Introduction

The amount of water contained in plant tissues is a key modulator of terrestrial ecosystem function. Plant water status can be quantified as vegetation water content (VWC) or as leaf water potential (ψ_l), which are monotonically related to each other in a given plant (Turner, 1988). During a drought, changes in VWC help determine whether plant mortality occurs and by what mechanism (i.e., carbon starvation or hydraulic failure) it tends to occur (Ding et al., 2021; Martinez-Vilalta et al., 2019; McDowell et al., 2008; Rao et al., 2019). VWC and ψ_l can also help predict how transpiration and photosynthesis respond to drought (Eller et al., 2020; Matheny et al., 2017). Each of these processes depends on plant water use strategy, which can be characterized by analyzing VWC and ψ_l dynamics (Konings & Gentine, 2017; Y. Liu, Konings, et al., 2021; Wu et al., 2021). VWC also reflects plant growth responses to rainfall pulses in semi-arid ecosystems (Feldman et al., 2021; Feldman, Short Gianotti,

Project Administration: Jeffrey D. Wood, Christian Frankenberg, Alexandra G. Konings
Resources: Yujie Wang, Jeffrey D. Wood, Christian Frankenberg, Alexandra G. Konings
Software: Nataniel Holtzman, Yujie Wang, Christian Frankenberg
Supervision: Alexandra G. Konings
Validation: Nataniel Holtzman, Yujie Wang, Jeffrey D. Wood, Christian Frankenberg, Alexandra G. Konings
Visualization: Nataniel Holtzman
Writing – original draft: Nataniel Holtzman
Writing – review & editing: Nataniel Holtzman, Yujie Wang, Jeffrey D. Wood, Christian Frankenberg, Alexandra G. Konings

et al., 2018) and modulation of land-atmosphere interactions (Feldman et al., 2020). Lastly, VWC dynamics strongly affect wildfire activity and burned area (Nolan et al., 2016; Rao et al., 2022; Yebra et al., 2013).

Global monitoring of VWC would improve our understanding of ecosystem resiliency and vulnerability to climate stress, especially considering that ecosystem responses to historical drought vary by region (Z. Yu et al., 2017), in part due to regional differences in the plant traits that modulate VWC dynamics. However, measurements of VWC and ψ_l are typically made in-situ on individual plants (Konings et al., 2019; Novick et al., 2022). It is difficult to scale these measurements up to coarser spatial scales with confidence, because of the high heterogeneity of plant traits within and across ecosystems (W. R. L. Anderegg, 2015; Skelton et al., 2015), within species (L. D. L. Anderegg et al., 2018; Garcia et al., 2022), and even between leaves on a individual plant (Proß et al., 2021). Remote sensing can help address this shortcoming, as data from spaceborne sensors are spatially widespread by design (Konings et al., 2021; Steele-Dunne et al., 2012). Out of the many wavelengths used for remote sensing, microwave observations are particularly sensitive to water content, both in the soil surface and in vegetation (Ulaby & Long, 2014).

The effect of vegetation moisture on microwave observables is typically characterized as vegetation optical depth (VOD), which is approximately linearly related to the total canopy water content in the area (Jackson & Schmugge, 1991). Total canopy water can be expressed as the product of aboveground biomass times VWC. In turn, through an ecosystem-scale (and ecosystem-specific) pressure-volume curve, VOD can be interpreted as an indirect indicator of ψ_l (Konings et al., 2019). Recent field and data-driven studies have shown that VOD is indeed sensitive to changes in leaf water potential on hourly, daily, and seasonal time scales (Holtzman et al., 2021; Momen et al., 2017). Depending on canopy structure, microwave observables such as VOD can also be sensitive to water in branches and/or stems, as well as leaves (Ferrazzoli & Guerriero, 1996; Holtzman et al., 2021). However, water potentials in leaves and other parts of an individual plant are closely related (Lambers et al., 2008), so VOD can be seen as an overall indicator of plant water potential, even if its sensitivity to specific vegetation components is not yet fully understood.

Based on the sensitivity of VOD to water potential in plants, VOD can be used as a constraint on plant hydraulics in a land surface model. In addition to aiding our ability to monitor and predict plant hydraulic responses to climate, such model-data fusion has been proposed as a way to estimate belowground water uptake, which is very difficult to measure directly (Konings et al., 2021; Y. Liu, Konings, et al., 2021). This approach is distinct from (and could be complementary to) assimilating VOD into an ecosystem model as a constraint on biomass (Kumar et al., 2020).

Y. Liu, Holtzman, and Konings (2021) fused satellite data with a simple land surface model to estimate globally resolved maps of plant hydraulic traits. That study found large between-trait differences in the ability of VOD data to constrain those traits. For example, the plant capacitance parameter was estimated with much more uncertainty than the g_1 parameter from the Medlyn stomatal conductance model. Many factors could contribute to these uncertainties, including the model accuracy, the inherent sensitivity of the model outputs to each trait, the prior distribution used for each trait in the model-data fusion algorithm, the observation operator that connects ψ_l with VOD (Shan et al., 2022), and the temporal availability of the remote sensing observations. It is unclear which factors are primarily responsible for the residual uncertainty and for the lack of constraint on certain traits.

Here, we investigate one avenue for potentially improving microwave remote sensing constraints on ecosystem dynamics: the temporal frequency of observations. Existing satellites carrying passive microwave sensors are typically in sun-synchronous orbits. This orbit type produces a repeat cycle where the satellite passes over a given point on Earth at two fixed times of day, 12 hr apart, such as for the Soil Moisture Active Passive (SMAP) mission (Entekhabi et al., 2010) and the Advanced Microwave Scanning Radiometer for EOS (AMSR-E) sensor (Kachi et al., 2014; Kim et al., 2018). These snapshots will rarely capture the full diurnal amplitude of leaf water potential, which tends to have a daily maximum just before dawn and daily minimum in early afternoon, approximately 8 hr apart (Katerji et al., 1986; Klepper, 1968). Nelson et al. (2018) found that the shape of the diurnal cycle of transpiration is an indicator of drought stress, which suggests that sub-daily VWC observations may enable improved characterization of drought stress. Such observations may also improve transpiration predictions, as many land surface models fail to capture the VWC-related hysteresis that has been observed in the diurnal cycle of transpiration relative to the cycles of vapor pressure deficit and solar radiation (Matheny et al., 2014; Renner et al., 2019). The degree of hysteresis is modulated partly by atmospheric variables (vapor pressure deficit and radiation), but also by vegetation hydraulic strategy and root-zone soil moisture, which could both potentially be constrained by passive microwave remote sensing (S. Xu et al., 2022; Zhang et al., 2014).

Unlike a sun-synchronous orbit, a geostationary orbit provides near-continuous observations in time (revisit time under 1 hr) over a fixed field of view. Geostationary satellites are widely employed for weather monitoring, but their data have also been recently used to constrain land surface processes (Khan et al., 2021). For example, T. Xu et al. (2018) estimated daily sensible and latent heat fluxes based on full diurnal cycles of land surface temperature (LST) from the Geostationary Operational Environmental Satellite (GOES) constellation. Xiao et al. (2021) provide an overview of upcoming geostationary satellite missions and their potential for studying ecosystem stress responses.

Konings et al. (2021) recently proposed two options for next-generation remote sensing of VWC: a geostationary satellite or a constellation of several small satellites (smallsats) with different orbits and thus different overpass times. The relevance of smallsat constellations to data assimilation is also discussed in Kumar et al. (2022). If eventually launched, the increased temporal resolution of these new mission concepts might improve our ability to constrain plant hydraulic traits and ecosystem dynamics. On the other hand, geostationary satellites are particularly expensive to engineer and launch since they orbit at a much greater distance from the Earth than satellites in sun-synchronous orbits. Thus, it is essential to determine how much benefit the increased information from possible new satellites would provide to scientific applications.

Here, we investigate that question: would observations throughout the day provide improved model performance and trait identification when fused with a land surface model? Or would they simply "connect the dots" in a consistent and predictable way between the existing twice-daily observations, providing no overall increase in information content? To quantify the potential utility of different observational frequencies, we use a simulation experiment. The simulation setting allows the sources of error in observations to be controlled, so that temporal frequency is the only difference between the experimental scenarios. We limit our focus here to passive microwave remote sensing (radiometry) rather than active (radar), because the physical processes relating VWC and remote sensing observables are better understood for radiometry than for radar (Konings et al., 2019; Shan et al., 2022).

In this study, we compare the utility of data that is available twice daily (analogous to a sun-synchronous orbit), four times daily (combining data from two satellites), or hourly (a geostationary orbit). We use Bayesian model-data fusion to infer plant hydraulic trait values from simulated remote sensing observations at these temporal frequencies. Because models with many parameters typically exhibit equifinality (Khatami et al., 2019; Tang & Zhuang, 2008) and because the observables are typically more sensitive to some parameters than other parameters, the accuracy of the retrieved trait values themselves does not tell the full story of whether the retrieved parameters accurately describe the ecohydrological system being studied. Thus, we also use the retrieved trait values to predict ecosystem responses to drought, focusing on soil moisture, evapotranspiration (ET) and gross primary productivity (GPP) as variables of interest. We analyze differences in the accuracy of these predicted ecosystem dynamics (relative to the original reference model run) across the different observational scenarios.

2. Materials and Methods

2.1. Experimental Design

Our study takes the form of an Observing System Simulation Experiment (OSSE), a simulation study in which retrieval algorithms are tested on simulated (but realistic) satellite observations to assess the accuracy of the environmental inference, which is associated with a known truth. The goal of an OSSE is to assess quantitatively how much information could be gained about an environmental process from a specific type of observation system (Arnold & Dey, 1986; Zeng et al., 2020). Since an OSSE is based on simulating both the observing system and the process being observed, it does not require that the observing system be operational yet, and thus can be used to plan future observing systems (Atlas, 1997). Here, we repeat the end-to-end OSSE simulation for several different scenarios associated with different observational frequency patterns, as further detailed below.

The steps in our OSSE are summarized in Figure 1. We started by running a land surface model (described in Section 2.2) to create simulated time series of ecosystem states and fluxes over 13 years (2005 through 2017) using meteorological forcing data from the Missouri Ozarks flux tower site (Wood & Gu, 2022). This model run used prescribed parameter values for plant and soil hydraulic traits, which were chosen to lead to realistic flux simulations compared to observations at the site. For the rest of the study, we then treated the parameter values and the associated states and fluxes from this model run as a synthetic "truth" scenario. We then used a

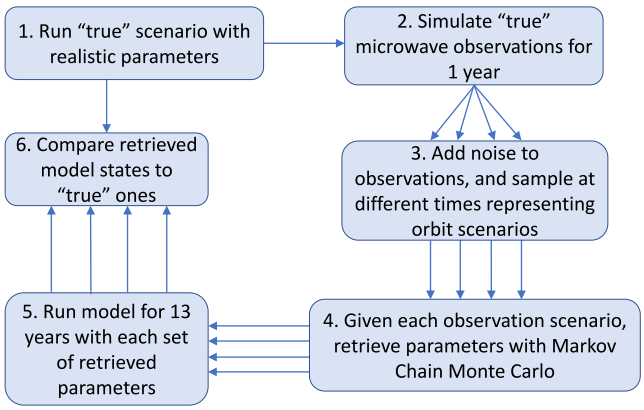

Figure 1. Schematic illustrating the overall framework of our simulation experiments. The sets of four parallel arrows represent the four observation scenarios.

radiative transfer model (described in Section 2.3) to simulate observations of horizontally and vertically polarized microwave brightness temperature for 1 year (2007), based on the land surface model outputs of surface soil moisture and vegetation water potential. Noise was added to these simulated brightness temperatures to mimic realistic levels of observational noise. The resulting simulated noisy brightness temperatures were then used in a Markov chain Monte Carlo (MCMC) algorithm (further described below) to estimate the underlying model parameters and their associated states and fluxes. These model parameters, states, and fluxes were then compared to the original assumed reference scenario to estimate the potential utility of brightness temperature observations.

We ran several parallel experiments, each with a different temporal arrangement of observations corresponding to a different satellite orbit scenario, determining the retrieved traits and associated fluxes for each scenario:

- "HOURLY"—observations 24 hr a day, every day (This represents a geostationary satellite.)
- "1 a.m./p.m."—observations at 1 a.m. and 1 p.m., every third day (This represents the approximate temporal resolution currently available from AMSR-E)
- "6 a.m./p.m."—observations at 6 a.m. and 6 p.m., every third day (This represents the approximate temporal resolution currently available from SMAP)
- "1 + 6"—combination of 6 a.m./p.m. and 1 a.m./p.m., with the four combined observations all coming on the same day of each 3-day cycle (This represents a combination of two satellites with different overpass times)

Figure 2 shows an example time series of VOD from the "true" model, and how each observation scenario views the same time series differently due to temporal frequency.

Based on each temporal subset of simulated observations over the 1-year observing period, we used a MCMC model-data fusion algorithm (described in Section 2.4) to retrieve Bayesian estimates of the land surface model parameters. For each scenario, we then took 120 samples from the estimated joint posterior distribution of parameters, and ran the land surface model for the full 13 years using each sampled parameter set. This procedure generates an ensemble of retrieved model runs that can be compared to the "true" model run. To illustrate the results of this methodology, Figure S1 in Supporting Information S1 shows the water potential over a few days for a subset of the retrieved ensemble.

Aside from the single year that was "observed" to retrieve the parameters, the 13-year evaluation period represents unseen inputs from the point of view of the retrieval algorithm. Evaluating the model behavior over this period is distinct from simply evaluating the accuracy of the retrieved parameters. Like real ecosystems, our model includes nonlinear processes that become especially important during drought; the xylem vulnerability curve is one example. In a year without climate stress, the effect of those processes on remote sensing observations of the ecosystem might be so small as to be masked by noise, so that observations during that year would not be useful for constraining the parameters governing those processes. We are interested in whether more frequent observations can help "unmask" those parameters. We intentionally did not include the most extreme drought year (2012) in the "observation" period, so that the model would have to predict ecosystem behavior under more extreme stress than it encountered when retrieving the parameters. This arrangement is relevant to practical applications, since ecosystem responses to extreme events are often of interest, but may not be present in the relatively short observational record and may become more likely with climate change (Frank et al., 2015; Reyer et al., 2013).

Over the evaluation period, we assessed the accuracy of several key model variables—leaf water potential (ψ_l), soil moisture, ET, and GPP—by calculating the root mean square error (RMSE) of each retrieved ensemble member relative to the "true" model run. In this analysis, we used the vertically integrated soil moisture over the entire soil column (2 m deep), not just the surface soil moisture that directly affects the microwave brightness temperature. For each observation scenario and each model variable, we obtained a probability distribution of RMSE over the posterior retrieved parameter distribution. We compared the RMSE distributions of the different

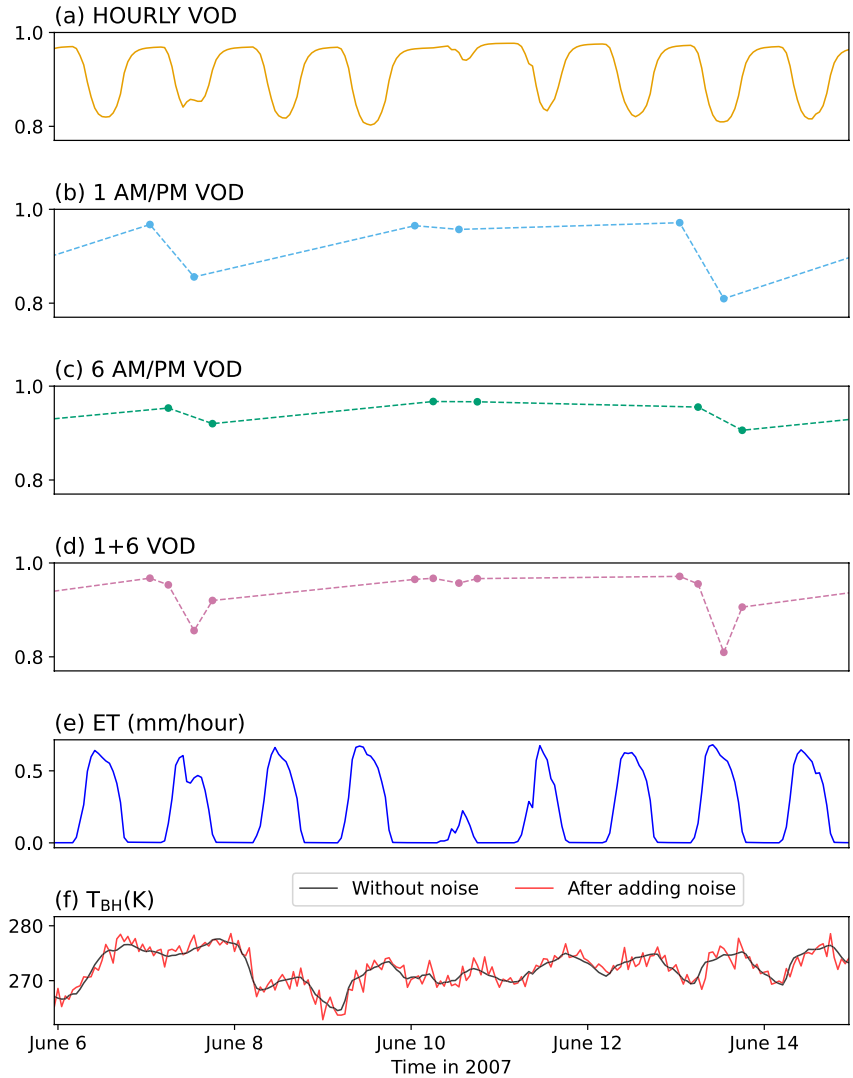

Figure 2. (a–d) Example time series of how the four observation scenarios sample vegetation optical depth (VOD) in time. (e) Model output evapotranspiration (ET) for reference. (f) Example of adding random noise to horizontally polarized brightness temperature (T_{BH}). Note that in our model-data fusion process, it is the noisy brightness temperatures, rather than VOD, which are directly combined with the model.

observation scenarios using a Mann-Whitney U test (a non-parametric analog to a *t*-test). We also calculated other error metrics (correlation and bias) to analyze the reasons for model performance differences between the observation scenarios.

In addition to predicting ecosystem behavior during typical conditions, it is also important to characterize responses to climate extremes. Thus, we repeated the RMSE analysis, but instead of using 13 full years in the error calculation, we limited the analysis to the four summers with the lowest total precipitation (aside from the 2007 model-data fusion year): 2005, 2012, 2013, and 2014. Here, summer was defined as 1 June through 30 September based on the growing season at the Missouri Ozarks site.

2.2. Model Structure

Previous work on using VOD to constrain plant hydraulics with model-data fusion has used simple models built specifically for that purpose (Y. Liu, Holtzman, & Konings, 2021). In the past few years, full-fledged land surface models—of the type that are used in global climate and weather modeling—have begun to include leaf water potential as a prognostic variable (Eller et al., 2020; Kennedy et al., 2019; L. Li et al., 2021), raising the

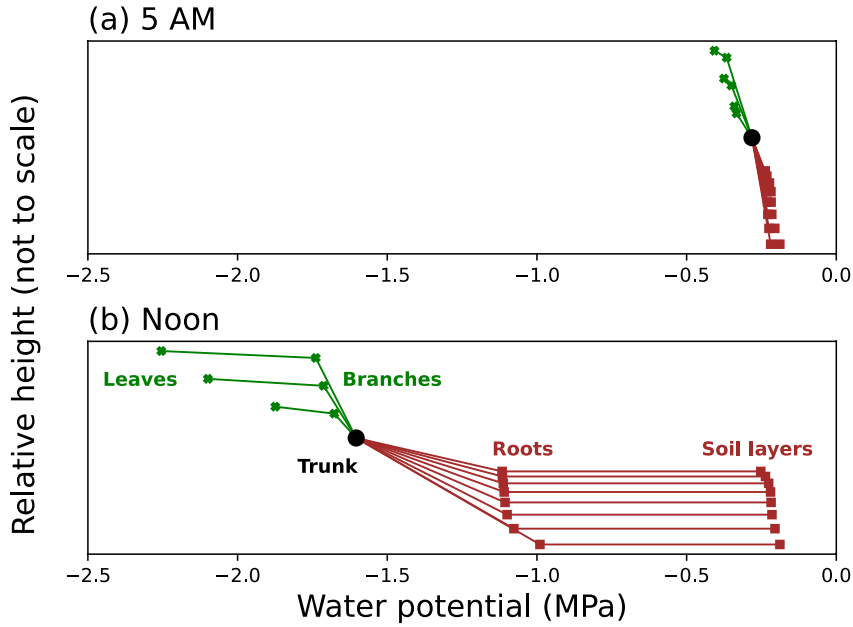

Figure 3. Schematic of plant organs as represented in Climate Modeling Alliance Land using sample, illustrative water potential values at two times of day.

possibility of using VOD to constrain the hydraulics of a land surface model. Here, we investigated model-data fusion in a new land surface model (Climate Modeling Alliance [CliMA] Land) that includes a sophisticated treatment of plant hydraulics (Y. Wang et al., 2023).

The land surface model used in this study is derived from the CliMA Land model, including the SoilPlantAirContinuum, Photosynthesis, and StomatalModels modules (Y. Wang et al., 2021). The model represents vegetation in analogy with a tree, with several organs: roots, trunk, branches, and leaves (Figure 3). The single trunk is connected at its base to several roots that extend down into different soil layers, and it is connected at its top to several branches that extend up to different heights. Each branch is connected to a leaf, and each leaf contains a sunlit part and a shaded part (not shown in Figure 3 for simplicity). Each canopy layer, comprising a branch and shaded/sunlit leaves, is connected to a layer of air. The model can contain an arbitrary number of canopy layers to model gradients of light within the canopy; however, in this study we only use three canopy layers for reasons of computational efficiency.

The processes and variables that are simulated prognostically in our model include: optical radiative transfer through the canopy, transpiration and photosynthesis in leaves, water potential and water content in each plant organ, water flow between connected plant organs, water uptake from soil to roots, vertical drainage through the soil, and runoff. Variables that are prescribed from external data include leaf area index (LAI), and meteorological data (precipitation, air temperature, humidity, and incoming solar radiation at the top of the canopy).

In each time step of the model, the following processes occur:

1. The transfer of light within the canopy is modeled based on incoming photosynthetically active radiation, LAI, and the vertical locations of leaf layers.
2. For each leaf layer, photosynthesis and stomatal conductance are modeled, yielding values of transpiration and carbon assimilation.
3. A non-steady-state plant hydraulics scheme models water flow, water storage, and water potential within the plant.
4. The soil moisture in each soil layer is updated to account for vertical drainage, precipitation, root water uptake, and runoff.

We added steps 3 and 4 specifically for the purposes of our study, beyond the SoilPlantAirContinuum module, while steps 1 and 2 are implemented similarly to the work of Y. Wang et al. (2021). We use a radiative transfer

model where each canopy layer has a sunlit fraction and a shaded fraction (Campbell & Norman, 1998). Photosynthetic carbon assimilation is modeled using the Farquhar model (Farquhar et al., 1980). Furthermore, in the photosynthetic step we attempted to mimic a realistic situation where the observational data contains processes that are not represented completely correctly in the model, by forcing the retrieval algorithm to work with a parametrization that is not completely representative of the "true" model. Specifically, we used two different stomatal conductance schemes: the "true" model uses the Medlyn scheme while the retrieval algorithm used the Ball-Berry scheme (Ball et al., 1987; Medlyn et al., 2011). This difference prevents the retrieval algorithm from being able to perfectly replicate the "true" model.

In Step 3 of the model, we implemented a new non-steady-state plant hydraulics scheme within CliMA Land. We introduce a capacitance-related parameter V (specifically, the total water volume stored by the plant at saturation). This parameter allows the model to represent a spectrum of possible plant hydraulic strategies beyond a simple steady-state assumption. Our scheme uses a governing equation based on Darcy's law, as in the FETCH2 plant hydraulic model (Mirfenderesgi et al., 2019; Silva et al., 2022). Unlike FETCH2, here we did not attempt to model gradients of water potential over the length of the vegetation components. Instead of a partial differential equation, our model is formulated as a system of ordinary differential equations, with one differential equation for each leaf, each branch, the trunk, and each root. Details of the plant hydraulic model and its linkage with stomatal function are described in Texts S1 and S2 in Supporting Information S1.

In Step 4 of the model, we use the Van Genuchten equation to parametrize the soil water retention curve and the Richards equation to model water drainage through the soil (Tindall et al., 1999; van Genuchten, 1980). There are eight soil layers in our model, with layer thicknesses increasing from top to bottom. The "true" model has a total soil depth of 2 m, with layer thicknesses ranging from 10 cm for the surface layer to 40 cm for the deepest layer. All soil properties such as porosity and saturated hydraulic conductivity are assumed to be homogeneous within the soil. A constant head boundary condition is assumed at the bottom of the soil column, as in the soil-plant-atmosphere continuum model of Y. Liu et al. (2017). Water runs off through saturation excess in the top layer and through drainage at the lower boundary. There is no spin-up period for soil moisture; the initial soil moisture is the same in all model runs (0.4 m^3/m^3 for all soil layers). At the beginning of each model run, vegetation water potential is initialized to be in equilibrium with the initial soil moisture.

2.3. Model Parameters

The model parameters that we retrieve from synthetic remote sensing observations are summarized in Table 1. Text S3 in Supporting Information S1 summarizes other model parameters that were not retrieved in this study but rather treated as known. Of the retrieved parameters, seven were related to plant traits and six were related to the soil. Our inclusion of a variety of soil parameters was motivated by the finding of Novick et al. (2022) that land surface model behavior is quite sensitive to soil parameter values. Furthermore, soil water retention curve parameters are not typically known a priori, but predicted from soil texture using pedotransfer functions that have large uncertainties (Novick et al., 2022; Vereecken et al., 2022).

The prescribed "true" values of the retrieved parameters were chosen to represent a temperate deciduous forest, using the rich ecological and physiological data available from the oak and hickory dominated Missouri Ozarks Ameriflux (MOFLUX) site to prescribe parameter values when possible (Gu et al., 2016; Wood et al., 2023). Soil depth was chosen to be 2 m; observed soil depths at the MOFLUX site range from 0.38 to 2 m (Wood & Gu, 2022). Using a deep rather than shallow soil for our "truth" scenario increases the challenge faced by the retrieval algorithm, since there is substantial decoupling in water content between the directly observed soil surface and the deeper soil layers. Soil hydraulic conductivity was chosen based on a typical value for the soil type found at the site, Weller silt loam soil (Young et al., 2001). The soil water retention curve was fitted to laboratory measurements on soil collected at the MOFLUX site (Wood et al., 2022).

The value of the maximum xylem water storage parameter was set using aboveground dry biomass estimates, based on the assumption that trees whose xylem is saturated with water contain approximately equal masses of dry matter and water. For maximum xylem water storage volume, we chose a value of 12 kg per square meter of ground area. This value comes from biomass data based on forest inventories at the Harvard Forest site in the northeastern US (Munger & Wofsy, 2020), which was assumed as a typical value for temperate deciduous forests in the US. Although there is not an overall biomass estimate for the Missouri Ozarks site, studies of other

Table 1
Parameters Retrieved From Simulated Observations

Parameter name and symbol	Units	Normalized by ψ_{ref}?	True value	Prior range
Remote sensing parameters				
Single scattering albedo (ω)	–	No	0.05	(0, ∞)
Sensitivity of VOD to leaf water potential (a)	MPa^{-1}	Yes	0.067	(0, ∞)
Contribution of woody biomass to VOD (b)	–	No	0.81	(0, ∞)
Sensitivity of VOD to LAI (c)	–	No	0.051	(0, ∞)
Stomatal parameters				
Maximum carboxylation rate (V_{cmax})	μmol/s per m^2 of leaf area	No	90	(10, 300)
g_1 in Medlyn model	$Pa^{1/2}$	No	300	N/A (see caption)
g_1 in Ball-Berry model	–	No	N/A	(1, 120)
$P63_\beta$	MPa	Yes	−3	(−0.75, −15)
Xylem parameters				
Whole-plant maximum xylem conductance (k_{plant})	mol/s/MPa per m^2 of basal area	Yes	10	(0.1, 50)
Whole-plant maximum water storage volume (V)	kg per m^2 of ground area	Yes	12	(0.12, 120)
$P63_x$	MPa	Yes	−4	(0.01,10) + $P63_\beta$
Soil parameters				
Soil depth (Z)	mm	No	2,000	(500, 3,000)
Soil moisture lower boundary condition (s_{lower})	m^3/m^3	No	0.4	(0.3, 0.5)
Rate of exponential decrease for rooting profile (α_{root})	m^{-1}	No	2	(0.01, 5)
Shape parameter of soil water retention curve (n)	–	No	1.5	(1.1, 1.9)
Water potential of soil with moisture of 0.21 (ψ_{ref})	MPa	N/A	−1	(−0.125, −8)
Saturated soil hydraulic conductivity (k_{soil})	μm/s	Yes	0.4	(0.05, 20)

Note. A flat non-negative prior is used for the remote sensing parameters. The other prior distributions are log-uniform. Note that the Medlyn model g_1 parameter is only used in the "true model," not in the retrieval, so it does not have a prior distribution. Also, $P63_x$ is parametrized in the MCMC as an additive constant plus the value of $P63_\beta$.

Missouri forests have found biomass ranging from 5 to 20 kg/m^2 (Chen et al., 2015; Hanberry et al., 2016; Q. Li et al., 2007).

Other parameter values were manually tuned so that the land model approximately matched the observed magnitude, seasonality, and interannual variation of ET, GPP, column-averaged soil moisture, and pre-dawn ψ_l at the MOFLUX site (Pallardy et al., 2018; Wood & Gu, 2022). Leaf area index (LAI) was prescribed as an input time series, though future versions of the CliMA model may include prognostic LAI within the model itself. We selected LAI data at the pixel over the MOFLUX site from the Moderate Resolution Imaging Spectrometer (MODIS) satellite (Myneni et al., 2002). We then adjusted the MODIS data's mean, amplitude, and seasonal timing to match in-situ LAI observations from the MOFLUX site. Because there were several time gaps in the in-situ LAI observations, we did not use them as direct inputs to CliMA.

Figure 4 demonstrates the model's realistic behavior by comparing model outputs with observed time series from eddy covariance and predawn ψ_l measurements. It should be noted that, as this study is an OSSE, our goal was not to perfectly calibrate a land surface model to a specific site, but rather to investigate model-data fusion with synthetic remote sensing data. We simply used the MOFLUX observations as a starting point to ensure the behavior of the new CliMA Land version was ecologically plausible.

2.4. Forward Model for Synthetic Remote Sensing Observations

Our synthetic simulation study used microwave brightness temperatures directly in the model-data fusion process, rather than using VOD and soil moisture data that has been retrieved from brightness temperature through an offline algorithm, to avoid errors due to any inaccuracies of such an algorithm. This approach is consistent with

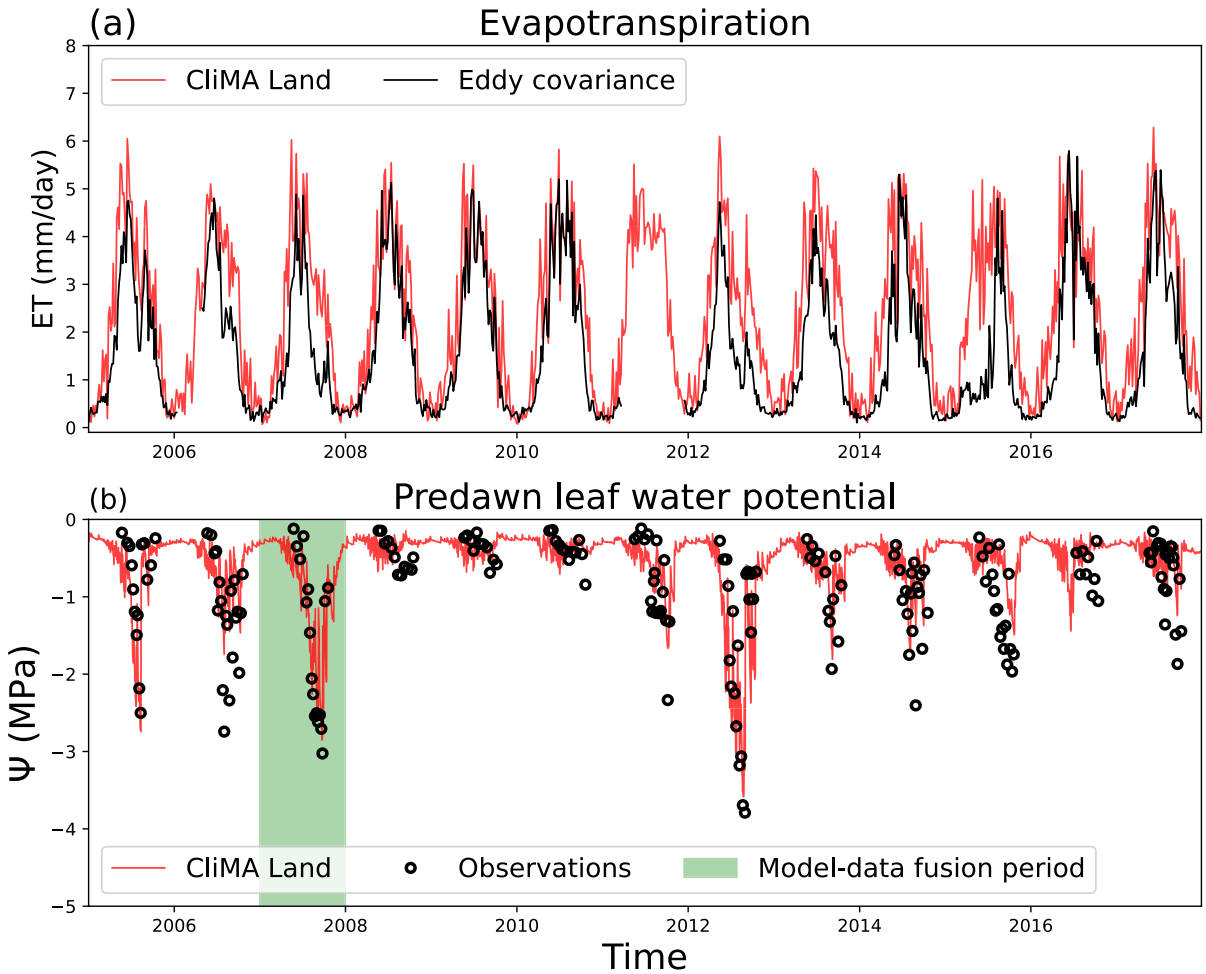

Figure 4. Comparison between "true" Climate Modeling Alliance (CliMA) Land simulation and observations at the Missouri Ozarks Ameriflux site for: (a) 5-day average evapotranspiration (ET), and (b) predawn leaf water potential. For reference, the 1-year model-data fusion period during which we used synthetic remote sensing observations is shown in green.

the notion of directly assimilating satellite observables instead of derived products, as advocated in two recent review papers (Kumar et al., 2022; MacBean et al., 2022). When using microwave data as a constraint on soil moisture, De Lannoy and Reichle (2016) found that it was advantageous to directly assimilate brightness temperatures into a land surface model, instead of assimilating soil moisture estimates derived from those brightness temperature. Here, we extended that concept to view brightness temperature as a joint constraint on soil moisture and plant hydraulics.

To simulate the propagation of microwaves near the land surface, we used the tau-omega zeroth-order radiative transfer model, which simulates brightness temperature T_B as a function of the soil surface dielectric constant and the VOD (Mo et al., 1982; Ulaby & Long, 2014), as described in the following equations:

$$T_B = \gamma(1 - r_s)T_s + (1 - \gamma)(1 + \gamma r_s)T_c \quad (1)$$

$$\gamma = \exp\left(-\frac{\text{VOD}}{\cos\,\theta}\right) \quad (2)$$

For a given polarization and viewing angle θ, the soil surface reflectivity r_s is determined by the soil's dielectric constant. We used the Mironov dielectric mixing model (Mironov et al., 2002) to parametrize the soil dielectric constant as a function of surface soil moisture output from the land model. The dielectric also depends on the clay content of the soil, which is 15% at the MOFLUX site and was treated as known for retrieval purposes

(Wood & Gu, 2022). The effect of surface roughness on the soil reflectivity is parametrized based on the SMAP algorithm (O'Neill et al., 2019) and also treated as known.

The single-scattering albedo, ω, is an important parameter in the radiative transfer model. Values of ω estimated from real satellite observations have considerable spatial variability even within land cover types (Konings et al., 2017). We thus treated ω as an unknown to be estimated from the observations. For the initial "truth" model, ω was set to 0.05, the value used by the SMAP algorithm for temperate deciduous forests (O'Neill et al., 2019). Calculating brightness temperature also requires the physical temperatures of the soil and canopy. In this study we assumed these temperatures are known with perfect accuracy from external data. Future versions of the CliMA Land model will include prognostic soil and canopy temperatures, which would enable bypassing that assumption by using physical temperature outputs from the model itself.

Plant water content affects microwave brightness temperature through VOD. We modeled VOD in the same way as several previous studies (Holtzman et al., 2021; Y. Liu, Holtzman, & Konings, 2021; Momen et al., 2017), as a function of leaf water potential (ψ_l, output by the land surface model) and LAI (prescribed by the forcing input data):

$$\mathrm{VOD} = (1 + a\psi_l)(b + c\mathrm{LAI}) \tag{3}$$

Above, a, b, and c are constant parameters, which vary between species and ecosystems. The first term, containing leaf water potential (ψ_l), represents VWC (and is mathematically equivalent to VWC here, since our plant hydraulic model assumes a linear pressure-volume curve). The second term, containing LAI, represents above-ground biomass (b represents the effect of woody biomass that does not change over time). As in Y. Liu, Holtzman, and Konings (2021), we treated these VOD parameters as unknowns to be estimated from microwave observations. Since CliMA Land represents an ecosystem comprised of multiple canopy layers and plant organs with differing water potentials, we must make an assumption about the layers/organs to which VOD is most sensitive. For example, in Equation 3, does ψ_l represent leaf water potential at the top of the canopy, averaged throughout the canopy, or some combination of leaf and stem water potential? Here, we used the average leaf water potential of the canopy layers, to represent short-wavelength microwave observations (e.g., X-band), which are relatively insensitive to the woody parts of vegetation (X. Li et al., 2021). However, further research on the relationship of VOD and ψ of different components is needed to determine the accuracy of this assumption.

The "true" VOD parameters (a, b, and c) were tuned to approximately match the local dynamics of remotely-sensed X-band VOD, using the Land Parameter Retrieval Model (LPRM) product based on data from the AMSR-E and AMSR2 satellites (Y. Y. Liu et al., 2011). At the scale of this data set's 51-by-29 km pixel size, the area of central Missouri immediately containing the MOFLUX site is a heterogeneous mix of forest and cropland, making its VOD difficult to interpret. Thus, to avoid representativeness error, we used LPRM data from a more homogeneously forested area in southeastern Missouri (Mark Twain National Forest, approximately 200 km away from MOFLUX) when tuning the "true" VOD parameters. A comparison of our model outputs with LPRM data is shown in Figure S2 in Supporting Information S1.

2.5. Retrieval Algorithm

To accomplish the inverse process of model-data fusion—estimating the model parameters that best match the observations—we used a MCMC approach. MCMC produces Bayesian estimates of model parameters, based on the likelihood of producing the observations given the parameters as well as prior probability distributions for the parameters. Compared to optimization methods that only retrieve point estimates of parameters, MCMC algorithms sample from the full joint distribution of parameters informed by data (the posterior distribution), permitting easier characterization of parameter trade-offs, equifinality, and uncertainty. The specific variety of MCMC algorithm we used was an Adaptive Metropolis-Hastings algorithm (Haario et al., 2001). Within the algorithm we normalized the log-likelihood of brightness temperature by the number of data points in each observation scenario, so that the only difference between scenarios is *when* the observations occur, not *how often* they occur.

We assumed that the observational noise in brightness temperatures follows a normal distribution with zero mean, a known standard deviation, and no temporal autocorrelation, and that the distribution of noise is identical and independent between the two polarizations. The standard deviation of the noise was set at 1.3 K, the observational

uncertainty of the SMAP radiometer (Chan et al., 2016). Figure 2f shows an example, for one polarization, of our simulated brightness temperature data before and after the addition of noise.

Within the MCMC algorithm, we reparametrized the model by log-transforming the land surface parameters, and also normalizing certain parameters; preliminary tests showed that without this normalization the MCMC chains converged much more slowly. For example, the parameter $P63_\beta$ is normalized by dividing it by the parameter ψ_{ref}, the water potential of soil with a volumetric moisture of 0.21 (the soil moisture that corresponds to a water potential of −1 MPa for the "true" model's water retention curve). The normalized parameters are labeled with a superscript circle, for example, $P63_\beta^o$. Furthermore, to compare values of leaf water potential in retrievals with greatly varying soil water retention curves, we also normalized ψ_l in a similar way. The normalization procedure is described in more detail in Text S4 in Supporting Information S1. The MCMC implementation is described in more detail in Text S5 in Supporting Information S1.

We only used 1 year of simulated observations in the model-data fusion process, rather than multiple years, due to the computational cost of the MCMC algorithm. We picked the year 2007 for this purpose because it includes substantial water stress, but not the highest water stress of the entire data set, which occurs in 2012.

3. Results

3.1. Comparison of Retrievals With Synthetic Observations

Fusing hourly synthetic brightness temperatures with the CliMA Land model effectively constrained VOD and surface soil moisture (the two retrieved variables that directly affect brightness temperature), as shown in Figure 5. Improved accuracy of the HOURLY posterior relative to the prior was evident in the overall mean value of the variables, their seasonal cycles, and their diurnal cycles over the model-data fusion year (2007). This success in model-data fusion occurred even though the "true model" VOD and surface soil moisture were far on the lower end of the prior distributions of those variables (Note that the prior distribution was not directly specified in terms of VOD or soil moisture, but rather in terms of the underlying model parameters that generate those time series). The relative difference in errors between the prior and the retrieval was much greater for VOD and surface soil moisture than it was for brightness temperature, because brightness temperature is also affected by the canopy and soil temperatures, which we treated as being known with perfect accuracy within the OSSE.

3.2. Parameter Retrievals

The HOURLY observation scenario showed the best parameter retrieval accuracy for several soil parameters, one xylem parameter, and for most of the remote sensing parameters, but not for other parameters (Figure 6). Parameters retrieved relatively accurately in all four observation scenarios include the scattering albedo, ω, and the xylem percentage loss of conductivity (PLC) curve parameter, $P63_x^o$ (Our model uses P63 due to representing PLC curves with a Weibull function; this P63 value can be converted to the more commonly measured P50 by multiplying by 0.83, or to P88 by multiplying by 1.46.). All four scenarios retrieved the total soil depth Z without much bias but with large uncertainty relative to the prior. For the three soil hydraulic parameters (Van Genuchten n, reference soil water potential ψ_{ref}, and soil saturated hydraulic conductivity k_{soil}^o), each was retrieved quite accurately in the HOURLY scenario, but had biases in the other scenarios. A similar pattern across scenarios was found with the VOD model parameters (a^o, b, and c) and the maximum plant water storage V^o. For the soil boundary condition s_{lower} and the rooting depth parameter α_{root}, the 1 a.m./p.m. scenario had a large bias while the other scenarios were more accurate. For the xylem conductance k_{plant}^o, the HOURLY scenario was most accurate, with the 1 + 6 scenario having a bias and the two twice-daily scenarios having a larger bias. All observation scenarios exhibited biases in retrievals of the stomatal parameters V_{cmax} and $P63_\beta^o$. This was to be expected due to our imposing the Ball-Berry stomatal model on the retrieval algorithm, in contrast to the Medlyn model used to generate the "true" data.

3.3. Accuracy of Retrieved Fluxes and Water States

Over the 13-year evaluation period, the HOURLY scenario was significantly more accurate in terms of daily-mean ψ_l than the two twice-daily scenarios are, but significantly less accurate than the 1 + 6 scenario (Figure 7a). A similar pattern held for ET (Figure 7c). The fact that the 1 + 6 scenario was *more* accurate for ψ_l and ET than the HOURLY scenario (despite having less data) suggests that the hourly observations contained times of day

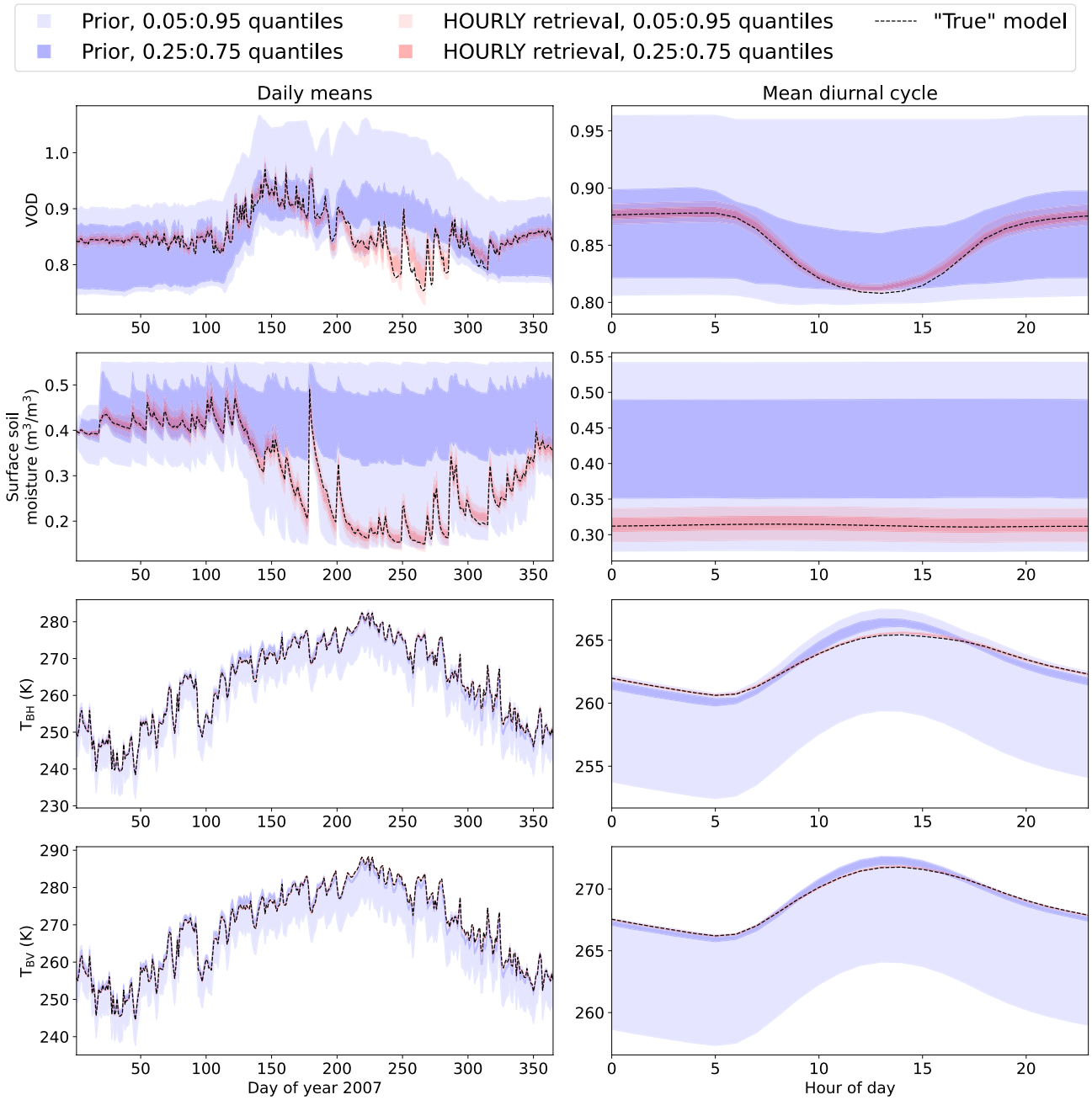

Figure 5. Comparison of vegetation optical depth, surface soil moisture, horizontally polarized brightness temperature (T_{BH}), and vertically polarized brightness temperature (T_{BV}) between the prior distribution, the HOURLY retrieval posterior distribution, and the true model, over the model-data fusion year 2007. For the prior and posterior distributions, the light shading represents the 0.05–0.95 quantile range, and the darker shading represents the 0.25–0.75 quantile range. Note that the "true model" brightness temperature data includes added random noise.

where brightness temperature is not informative of plant hydraulics. Since the likelihood calculations in each scenario were normalized by the number of observations, the addition of these superfluous times of day apparently hurt the overall accuracy of the HOURLY scenario.

For column-averaged soil moisture, the HOURLY scenario was significantly more accurate than the other scenarios (Figure 7b). This finding highlights the potential for diurnal observations to improve our estimation of multiple land surface variables, even those like soil moisture that do not change much over a single day themselves, but are influenced by variables like ET that *do* exhibit strong diurnal variation. Finally, for GPP, the twice-daily

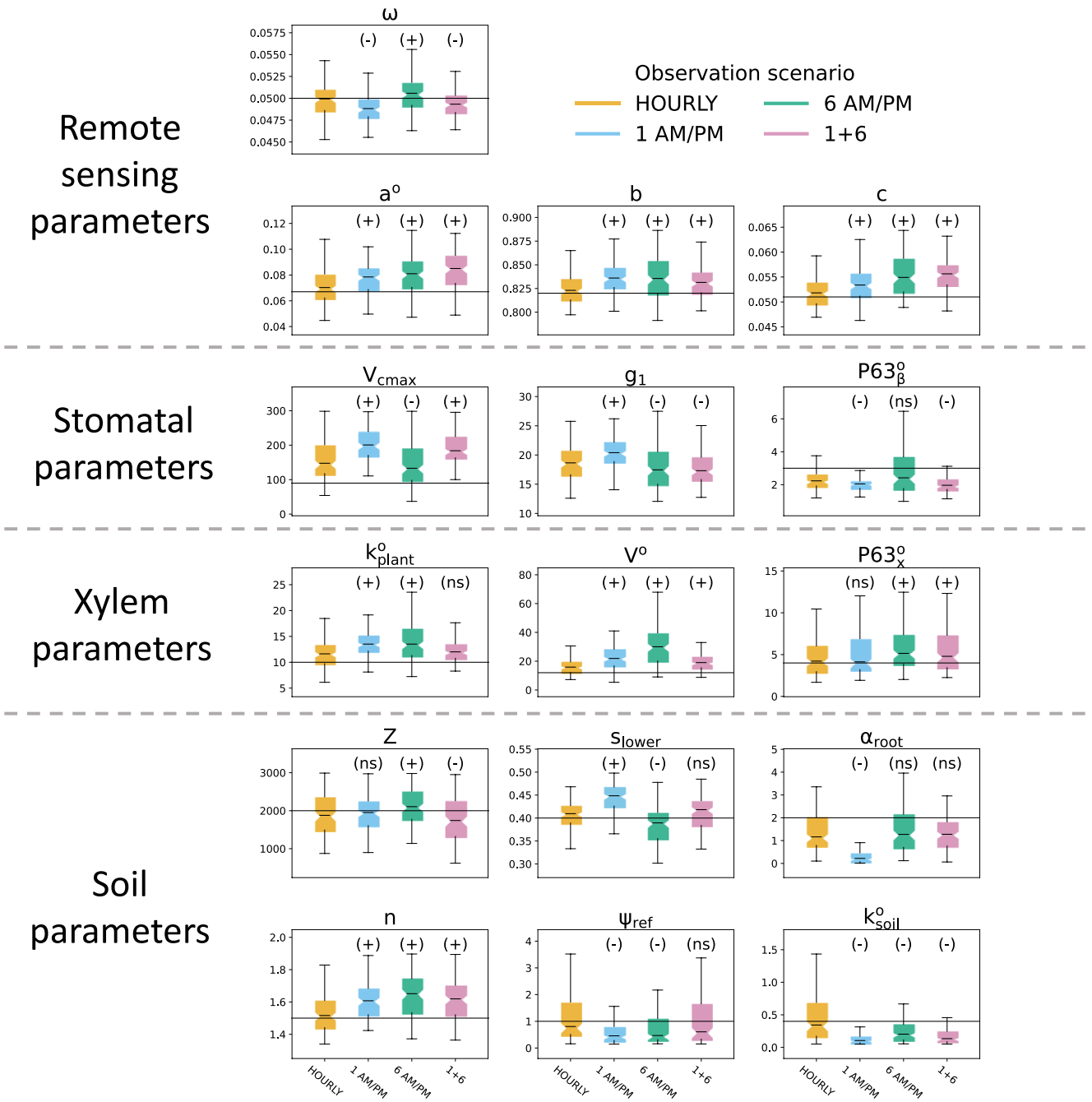

Figure 6. Posterior distributions of retrieved parameters under four observing scenarios. For each sub-panel, the black horizontal line is the "true" value, except for g_1, which does not have a "true" value because the retrievals use a different stomatal model from the "true" model run. See Table 1 for the units of each parameter. Parameters with names marked with a superscript "o" have been normalized by the value of ψ_{ref}, as described in Text S4 in Supporting Information S1. The symbols in parenthesis above the individual boxes represent statistical significance of the differences between scenarios, calculated with a Mann-Whitney U test using the HOURLY scenario as a baseline. A "(+)" mark represents significantly higher parameter values compared to the "hourly" scenario; a "(−)" mark represents significantly lower parameter values; a "(ns)" mark represents no significant difference ($p > 0.05$).

scenarios were significantly less accurate than the hourly one, while the 1 + 6 scenario has similar accuracy to the HOURLY one (Figure 7d). Similar patterns of RMSE differences between observation scenarios were found when we calculated RMSE based on hourly model outputs instead of daily averages (Figure S3 in Supporting Information S1).

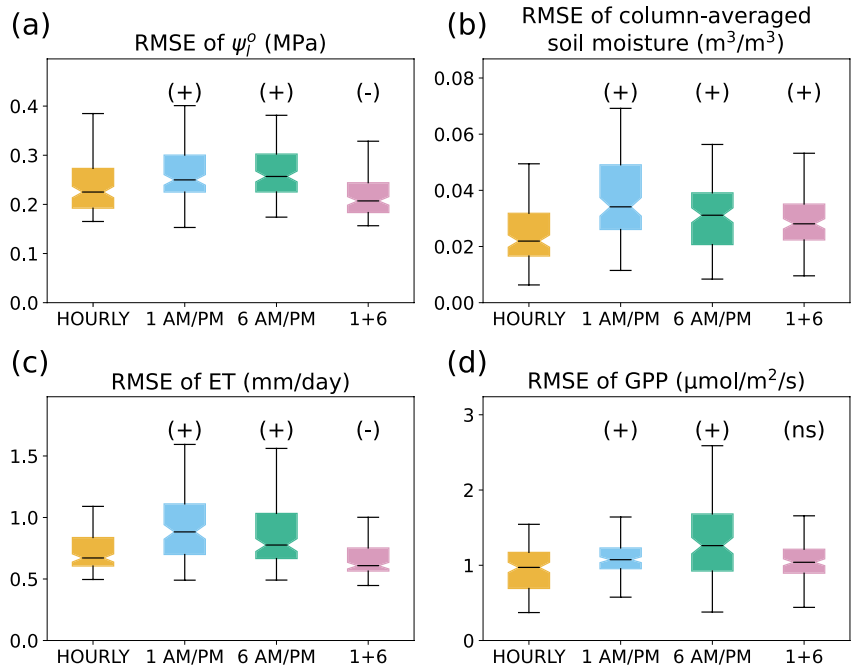

Figure 7. Box plots showing posterior distributions of root mean square error (RMSE) for daily-averaged variables *over entire evaluation period*: (a) normalized leaf water potential, (b) column-averaged soil moisture, (c) evapotranspiration, (d) gross primary productivity (GPP). Note that leaf water potential is normalized with respect to the soil water retention curve, as discussed in Text S4 in Supporting Information S1. The symbols in parenthesis above the individual boxes represent statistical significance of the differences between scenarios, calculated with a Mann-Whitney U test using the HOURLY scenario as a baseline. A "(+)" mark represents significantly *greater* RMSE (i.e., worse model performance) compared to the "hourly" scenario; a "(−)" mark represents significantly *smaller* RMSE (i.e., better performance); a "(ns)" mark represents no significant difference in RMSE ($p > 0.05$).

The qualitative pattern of differences between observation scenarios over the driest summers was similar to the pattern over the entire 13-year period (Figure 8). However, between-scenario differences in ET and GPP accuracy were larger in magnitude over these driest summers than over the entire 13-year period. Over the 13-year evaluation period, the posterior median RMSE of ET was 45% greater for the 1 a.m./p.m. (worst) scenario than for the 1 + 6 scenario, while over the four driest summers the corresponding difference was 91%. Similarly for GPP, over the 13-year evaluation period, the posterior median RMSE was 21% greater for the 6 a.m./p.m. (worst) scenario than for the 1 + 6 scenario, while over the four driest summers the corresponding difference was 77%.

3.4. Drivers of Differences Between Observational Scenarios

To examine the reasons why some observation scenarios perform better than others, we broke down ψ_l errors into the RMSE of predawn ψ_l (specifically 5 a.m.) and the RMSE of ψ_l diurnal amplitude (Figures 9a and 9b). Here, diurnal amplitude was calculated as the difference of the 5 a.m. value minus the 2 p.m. value, where we assume based on an average diurnal cycle that 5 a.m. is near the diurnal maximum and 2 p.m. is near the diurnal minimum. We also calculated additional error metrics for ET: bias and Pearson correlation (Figures 9c and 9d). This analysis was performed only over the model-data fusion year (2007). If we considered the entire 13-year evaluation period, it would be more likely that errors in one variable would "spill over" into other variables, leading to uncertainty over which variable is the root cause of inaccuracy.

The 1 a.m./p.m. scenario was by far the least accurate at retrieving pre-dawn leaf water potential (Figure 9a). This failure was presumably due to lack of observations during the predawn period when the soil and vegetation are closest to hydraulic equilibrium. The 1 a.m./p.m. scenario thus could not constrain root-zone dynamics, and retrieved an inaccurately deep rooting depth (smaller α_{root}), with considerably greater error than in the other scenarios (Figure 6). Due to this failure, the 1 a.m./p.m. scenario predicted significantly higher ET than the

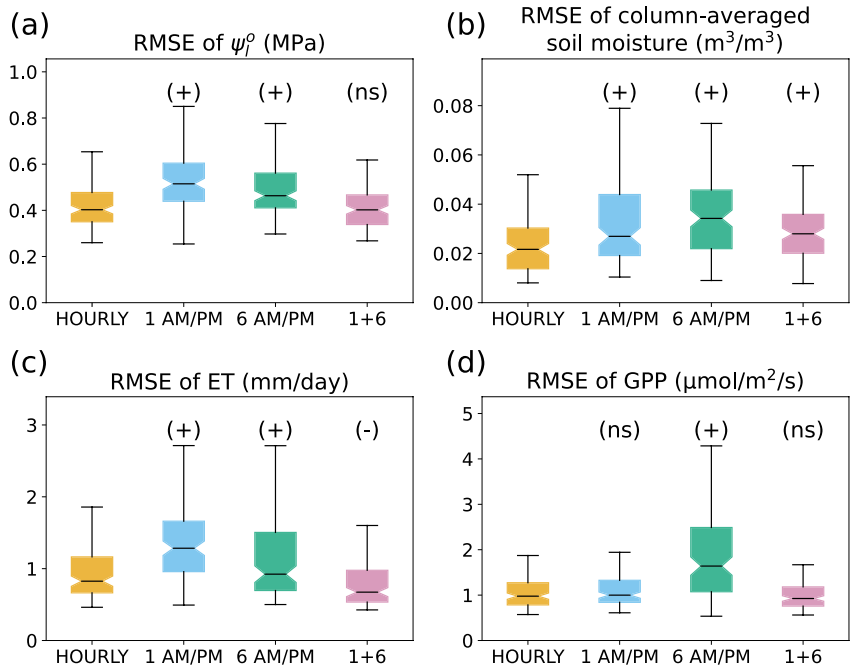

Figure 8. Box plots showing posterior distributions of root mean square error (RMSE) for 4 daily-averaged variables *over the four summers with the least precipitation*. Note that leaf water potential is normalized with respect to the soil water retention curve, as discussed in Text S4 in Supporting Information S1. The symbols in parenthesis above the individual boxes represent statistical significance of the differences between scenarios, calculated with a Mann-Whitney U test using the HOURLY scenario as a baseline. A "(+)" mark represents significantly *greater* RMSE (i.e., worse model performance) compared to the "hourly" scenario; a "(−)" mark represents significantly *smaller* RMSE (i.e., better performance); a "(ns)" mark represents no significant difference in RMSE ($p > 0.05$).

true model (Figure 9c) and had the largest RMSE in column-averaged soil moisture among the four scenarios (Figure 7b).

By contrast, the 6 a.m./p.m. scenario did especially poorly at capturing the diurnal amplitude of leaf water potential (Figure 9c). This inaccuracy may be explained by the fact that the 6 a.m./p.m. scenario did not contain observations during the midday peak of water stress. The 6 a.m./p.m. scenario also had the lowest Pearson correlation with the "true" ET, indicating that the 6 a.m./p.m. retrieval did not model the temporal dynamics of ET correctly. This failure may be due to inaccurate representation of water stress and stomatal closure, resulting from the lack of observations during water-stressed hours. The $P63_\beta$ parameter (which regulates under what conditions water stress occurs) was less tightly constrained in the 6 a.m./p.m. retrieval than in other retrievals (Figure 6). The 6 a.m./p.m. scenario's inaccuracy in predicting GPP (Figures 7d and 8d) may also be related to its lack of observations of the midday period when GPP is highest within a day.

Combining 1 a.m./p.m. observations and 6 a.m./p.m. observations remedied the above issues with both individual observational scenarios. The 1 + 6 scenario predicted ET, GPP, and soil moisture significantly more accurately than in either twice-daily scenario alone (Figures 7b–7d, 8b–8d, 9c[7b–7d], and 9d). This finding is not surprising, given that the 1 + 6 scenario is based on more observations. Our more important finding is that the 1 + 6 scenario has similar accuracy to the HOURLY scenario.

4. Discussion and Conclusions

4.1. Prospects for Constraining Plant Water Stress Response From Remote Sensing

The observing scenarios analogous to a sun-synchronous orbit, with two observations per day every 3 days, provide a significantly worse constraint on modeled states and fluxes relative to the "geostationary" or "HOURLY" scenario. As discussed in Section 3.3, the two twice-daily scenarios perform poorly for different reasons related to their specific overpass times. However, combining observations from both of the sun-synchronous orbits

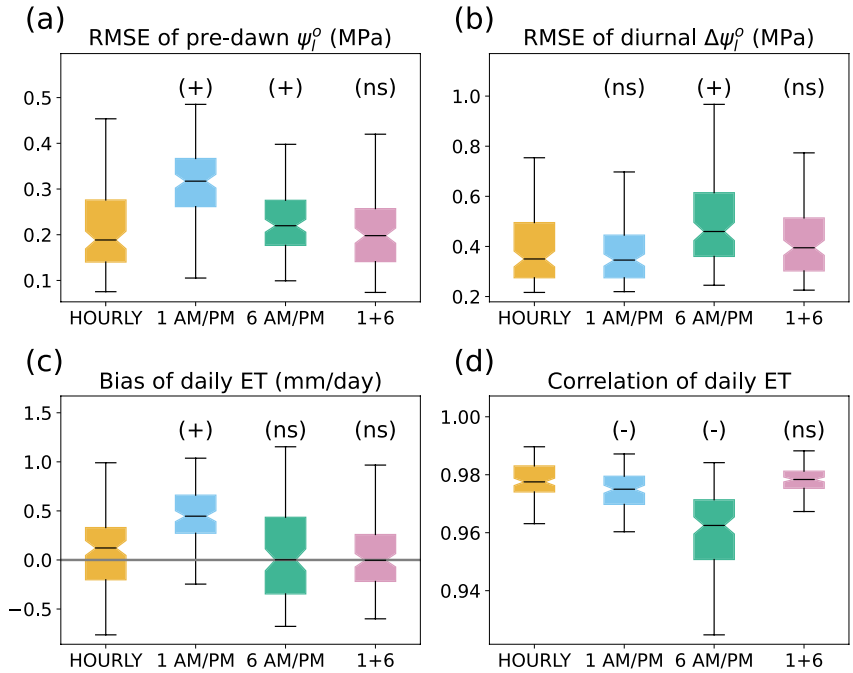

Figure 9. Box plots showing posterior distributions of several error metrics *during the model-data fusion year (2007)*: (a) root mean square error (RMSE) of 5 a.m. normalized leaf water potential, (b) RMSE of the diurnal amplitude of normalized leaf water potential (5 a.m. minus 2 p.m.), (c) bias of daily evapotranspiration (ET), (d), correlation of daily ET. Note that leaf water potential is normalized with respect to the soil water retention curve, as discussed in Text S4 in Supporting Information S1. The symbols in parenthesis above the individual boxes represent statistical significance of the differences between scenarios, calculated with a Mann-Whitney U test using the HOURLY scenario as a baseline. A "(+)" mark represents significantly greater values compared to the "hourly" scenario; a "(−)" mark represents significantly smaller values; a "(ns)" mark represents no significant difference in values ($p > 0.05$).

(6 a.m./p.m. and 1 a.m./p.m.) constrained the model fluxes with similar accuracy to the HOURLY scenario. It appears that, at least in our case study, the most significant diurnal fluctuations in ψ_l can be inferred with reasonable accuracy from snapshots of brightness temperature at four adequately-spaced times of day, but not from just two times of day. Consistent with these variations, the vegetation capacitance was well constrained in the HOURLY and 1 + 6 scenarios, but not in the 1 a.m./p.m. or 6 a.m./p.m. scenarios. As illustrated in Figure S4 in Supporting Information S1, the capacitance parameter affects the shape of the VWC diurnal cycle (e.g., how quickly the xylem refills at night), which may explain why more frequent sub-daily observations improve capacitance constraints. By contrast, the plant-hydraulic model data fusion study of Y. Liu, Holtzman, and Konings (2021) found only limited ability to constrain vegetation capacitance with sun-synchronous observations from AMSR-2 alone.

In our study, model-data-fusion enhances modeled root-zone soil moisture accuracy, providing support for the idea that remote sensing of VWC could provide increased understanding of root-zone soil conditions. When sampling from the prior parameter distributions without any data constraints, the median RMSE of column-averaged soil moisture is 0.093 m^3/m^3 (not shown). The corresponding value even for the worst-performing model-data-fusion scenario (1 a.m./p.m.) is 0.034 m^3/m^3—a 2.7x decrease in error. This improvement occurs even though the soil parameters were less tightly constrained relative to their priors than the plant hydraulic parameters (Figure 5). In the future, additional simulation experiments could be performed to distinguish how much of this improvement is due to brightness temperatures' sensitivity to surface soil moisture or to VWC. For example, would our results still hold in an ecosystem whose value of the a parameter in Equation 3 (sensitivity of VOD to leaf water potential) was smaller than that assumed here?

4.2. Retrieval Accuracy Is on Par With That of Other Land Surface Data Assimilation Efforts

To put the results of our OSSE in a broader context, we can compare the errors in model states and fluxes we found here with error metrics in other studies where remote sensing or site-level data was used to constrain a land surface model. It should be expected that our study will have lower errors than comparisons with observational data, since the only sources of differences between "true" and retrieved data in our study are the noise in brightness temperatures and the intentionally incorrect stomatal conductance scheme. Assimilation studies using observational data contain additional model structural errors, inaccuracies in the forcing data such as precipitation and radiation, and potentially scaling errors between remotely sensed data and in-situ data. However, the comparison can at least provide a qualitative perspective on how much error is due to observational noise (the primary source of error simulated here) relative to other sources or inaccuracy. Here, we compare error metrics for two variables in our study with two observational data assimilation studies: Reichle et al. (2017) for root-zone soil moisture and Y. Wang et al. (2021) for ET.

Reichle et al. (2017) compared the SMAP L4 root zone soil moisture product with in-situ measurements from 17 validation sites in grasslands, savannas, and croplands with a range of soil types, using soil moisture sensors between 0.45 and 0.75 m deep. The SMAP L4 product is derived by assimilating SMAP brightness temperatures into the Catchment land surface model using an ensemble Kalman filter instead of the Bayesian model-data-fusion method used here. For root zone moisture, that study found unbiased RMSE (ubRMSE, found by removing additive bias before calculating RMSE) values of approximately 0.025–0.03 m^3/m^3 and correlations (R) of 0.7–0.85. In our study, column-averaged soil moisture ubRMSE ranged between 0.015 and 0.028 m^3/m^3 for the four observing scenarios and R ranged between 0.91 and 0.97 (These metrics are calculated at a 3-hr time resolution to match the SMAP L4 study). The approximate similarity in soil moisture error ubRMSE between our study and the SMAP L4 product provides some confidence that our study realistically represents data assimilation of passive microwave remote sensing of soil moisture. Our substantially higher R values are probably a result of our experiment using the same forcing data for the "true" model and retrievals.

Y. Wang et al. (2021) calibrated the CliMA model (without the modifications discussed in Section 2.2) to match measured ET and net ecosystem exchange at the MOFLUX site. Their best-performing model setup had a mean absolute standardized error (MASE) of 29% for half-hourly ET during the growing season. MASE is calculated by dividing mean absolute error by the standard deviation of the observed or "true" data. In our study, the median growing-season MASE of hourly ET for each of the five observation scenarios relative to the "true model" ranged from 15% to 25% across scenarios. The similarity in MASE between our simulation study and Wang et al.'s real-data comparison builds additional confidence that our simulations remain close to what might be expected in a true observational scenario, despite the various idealizing assumptions.

4.3. Limitations of This Study

Several assumptions and simplifications in our methodology should be acknowledged. First, our entire study is based on one site and one set of "true" parameters. A follow-up study could extend our approach to multiple sites with different plant functional types and climatic conditions, and/or include multiple values of prescribed "true" parameters to retrieve. Second, we only tested one assumption about which plant components contribute to VOD (leaves, but not branches or stems). The relative contributions of different plant components to VOD may differ by wavelength and by plant type (Ferrazzoli & Guerriero, 1996). Additionally, since VOD measures total canopy water, it be affected by water on the surface of leaves (canopy interception and dew), which is not currently considered in the CliMA model. Studies that have examined the effect of this canopy surface water on microwave remote sensing observables have variously found large effects (Khabbazan et al., 2022; X. Xu et al., 2021), small and potentially negligeable effects (Hornbuckle et al., 2007), or no measurable effect (Escorihuela et al., 2009; Holtzman et al., 2021). Whether canopy surface water can be ignored while studying VOD presumably depends on local conditions including leaf area and canopy structure (smaller leaves would intercept less water), and how often meteorological conditions favorable for dew occur.

We did not explore the full possible spectrum of complexity in the radiative transfer model. First, we assumed a particular and relatively simple relationship between leaf water potential, VWC, and VOD. More physically detailed parametrizations of the VWC-VOD relationship have recently been proposed (Fink et al., 2018; Humphrey & Frankenberg, 2023), as well as alternative empirical models to Equation 3 (Forkel et al., 2023).

Second, we treated the VOD model coefficients (a, b, and c) and the scattering albedo ω as constant over time. However, in many ecosystems the scattering albedo van vary significantly over time with seasonal and interannual changes in vegetation structure (Baur et al., 2021; Konings et al., 2016; H. Wang et al., 2023). Third, we treated the effect of soil roughness on brightness temperature at our site as known a priori, when it varies spatially. Pixel-wise tuning of the roughness parametrization has been shown to reduce radiative transfer model biases in the context of passive microwave data assimilation (Lievens et al., 2015). A more realistic treatment of the roughness parametrization would also vary in time, since the roughness parametrization implicitly accounts for leaf litter, which interacts differently with microwaves when the litter is wet (after rainfall) from when it is dry (Kurum et al., 2012; Wigneron et al., 2017). Finally, the tau-omega radiative transfer model we used does not account for multiple scattering by vegetation, which can lead to errors when used in very dense forests where more complicated radiative transfer models are more appropriate (Ambadan et al., 2022; Feldman, Akbar, & Entekhabi, 2018).

Another simplification we made was our assumption of perfect knowledge of soil and canopy temperatures throughout the day (these physical temperatures are used in relating VOD and surface soil moisture to microwave brightness temperatures). Future versions of the CliMA model will have prognostic soil and canopy temperatures, which would allow brightness temperature to be used as a constraint without requiring external soil/canopy temperature data, as is done in other land surface models (Han et al., 2014; Reichle et al., 2017). One challenge with this approach is that the difference between air and canopy temperatures is highly variable by time of day and vegetation type (Javadian et al., 2022; Still et al., 2022).

Remotely sensed LST itself is available at high temporal resolution from geostationary satellites such as GOES and the Spinning Enhanced Visible and Infrared Imager (Sun & Pinker, 2003; Y. Yu et al., 2012). The combination of LST and microwave brightness temperature can be used to jointly constrain a land surface model (Lu et al., 2017). It is possible that some of the benefit of frequent microwave observations found in our study could also be realized from combining twice-daily microwave data with hourly LST. Simultaneously assimilating additional forms of remote sensing data might also be useful, such as solar induced fluorescence which is linked to photosynthesis and thus GPP (Norton et al., 2019).

4.4. Implications for Satellite Missions

Our findings are encouraging for efforts to estimate ecosystem carbon and water fluxes and plant hydraulic traits by fusing existing satellite data with plant hydraulics-enabled land surface models (with the caveat that vegetation trait values retrieved from model-data fusion are specific to the land surface model used, and would be expressed at the scale of satellite pixels). Based on the good performance of the four-times-daily scenario, combining data from multiple microwave satellites, with overpass times covering both pre-dawn and mid-day, should be beneficial to model-data-fusion efforts. It is also likely to be beneficial for model validation and parametrization efforts, which should similarly benefit from the information encoded in such observations. The exact size of the accuracy boost from increased observations per day might vary between ecosystems. For example, we might expect differences between temperate forests like our study site, grasslands with lower overall VOD than our study site, and tropical rainforests with less frequent water stress than our study site. However, our overall results should qualitatively hold for any ecosystem in which the diurnal cycle of plant water content is strong enough to influence VOD.

The benefits of four-times-daily data may even be achievable with currently operating satellite missions. However, there are additional challenges associated with data fusion from multiple satellites. Post-processing and careful uncertainty analysis would be required to co-locate the data from sensors with different spatial resolutions onto a common grid. Also, sensors operating in different wavelengths typically have differing effective penetration depths through the canopy, so the effect of VWC on VOD differs by sensor, necessitating a separate observation operator for each sensor in the model-data-fusion process. These factors were not considered in our study, where we assumed the 6 a.m./p.m. and 1 a.m./p.m. overpasses interacted with the vegetation in identical ways. Nevertheless, if between-sensor differences can be accounted for, using data from both SMAP and AMSR2 as a constraint, for example, should provide a significant boost in trait accuracy and modeled fluxes compared to only using observations from one microwave sensor. In fact, combining data from sensors with different wavelengths could help partition VWC between different sections of the canopy (e.g., leaves vs. woody biomass) due to the contrasting penetration depths of the sensors.

Data Availability Statement

All code used in this project is available in a GitHub repository: https://github.com/natan-holtzman/CliMa_Microwave.

The repository includes source code for our version of the CliMA Land model, meteorological data used as model forcing, MCMC code for the retrieval algorithm, and scripts to analyze the model outputs and produce the figures in this paper.

The following Zenodo repository contains retrieved posterior parameter distributions, and posterior quantiles for the retrieved time series of model states and fluxes: https://doi.org/10.5281/zenodo.7757684.

Acknowledgments
NH is supported by a Future Investigators in NASA Earth and Space Science and Technology (FINESST) Grant (80NSSC20K1620) from the National Aeronautics and Space Administration (NASA). NH, AGK, JDW, and CF are supported by the NASA Carbon Cycle Science program (80NSSC21K1712). NH and AGK are also supported by NSF DEB-1942133. YW and CF gratefully acknowledge the generous support of Eric and Wendy Schmidt (by recommendation of the Schmidt Futures initiative) and the Heising-Simons Foundation.

References

Ambadan, J. T., MacRae, H. C., Colliander, A., Tetlock, E., Helgason, W., Gedalof, Z., & Berg, A. A. (2022). Evaluation of SMAP soil moisture retrieval accuracy over a boreal forest region. *IEEE Transactions on Geoscience and Remote Sensing*, *60*, 1–11. https://doi.org/10.1109/TGRS.2022.3212934

Anderegg, L. D. L., Berner, L. T., Badgley, G., Sethi, M. L., Law, B. E., & HilleRisLambers, J. (2018). Within-species patterns challenge our understanding of the leaf economics spectrum. *Ecology Letters*, *21*(5), 734–744. https://doi.org/10.1111/ele.12945

Anderegg, W. R. L. (2015). Spatial and temporal variation in plant hydraulic traits and their relevance for climate change impacts on vegetation. *New Phytologist*, *205*(3), 1008–1014. Article 3. https://doi.org/10.1111/nph.12907

Arnold, C. P., & Dey, C. H. (1986). Observing-systems simulation experiments: Past, present, and future. *Bulletin of the American Meteorological Society*, *67*(6), 687–695. https://doi.org/10.1175/1520-0477(1986)067<0687:OSSEPP>2.0.CO;2

Atlas, R. (1997). Atmospheric observations and experiments to assess their usefulness in data assimilation. *Journal of the Meteorological Society of Japan. Series II*, *75*(1B), 111–130. https://doi.org/10.2151/jmsj1965.75.1B_111

Ball, J. T., Woodrow, I. E., & Berry, J. A. (1987). A model predicting stomatal conductance and its contribution to the control of photosynthesis under different environmental conditions. In J. Biggins (Ed.), *Progress in photosynthesis research* (pp. 221–224). Springer Netherlands. https://doi.org/10.1007/978-94-017-0519-6_48

Baur, M. J., Jagdhuber, T., Feldman, A. F., Chaparro, D., Piles, M., & Entekhabi, D. (2021). Time-variations of zeroth-order vegetation absorption and scattering at L-band. *Remote Sensing of Environment*, *267*, 112726. https://doi.org/10.1016/j.rse.2021.112726

Campbell, G. S., & Norman, J. M. (1998). *An introduction to environmental biophysics*. Springer. https://doi.org/10.1007/978-1-4612-1626-1

Chan, S. K., Bindlish, R., O'Neill, P. E., Njoku, E., Jackson, T., Colliander, A., et al. (2016). Assessment of the SMAP passive soil moisture product. *IEEE Transactions on Geoscience and Remote Sensing*, *54*(8), 4994–5007. Article 8. https://doi.org/10.1109/TGRS.2016.2561938

Chen, J., Xu, J., Jensen, R., & Kabrick, J. (2015). Changes in aboveground biomass following alternative harvesting in oak-hickory forests in the eastern USA. *iForest: Biogeosciences and Forestry*, *8*(5), 652–660. https://doi.org/10.3832/ifor1349-007

De Lannoy, G. J. M., & Reichle, R. H. (2016). Global assimilation of multiangle and multipolarization SMOS brightness temperature observations into the GEOS-5 catchment land surface model for soil moisture estimation. *Journal of Hydrometeorology*, *17*(2), 669–691. https://doi.org/10.1175/JHM-D-15-0037.1

Ding, Y., Nie, Y., Chen, H., Wang, K., & Querejeta, J. I. (2021). Water uptake depth is coordinated with leaf water potential, water-use efficiency and drought vulnerability in karst vegetation. *New Phytologist*, *229*(3), 1339–1353. https://doi.org/10.1111/nph.16971

Eller, C. B., Rowland, L., Mencuccini, M., Rosas, T., Williams, K., Harper, A., et al. (2020). Stomatal optimization based on xylem hydraulics (SOX) improves land surface model simulation of vegetation responses to climate. *New Phytologist*, *226*(6), 1622–1637. https://doi.org/10.1111/nph.16419

Entekhabi, D., Njoku, E. G., O'Neill, P. E., Kellogg, K. H., Crow, W. T., Edelstein, W. N., et al. (2010). The soil moisture active passive (SMAP) mission. *Proceedings of the IEEE*, *98*(5), 704–716. Article 5. https://doi.org/10.1109/JPROC.2010.2043918

Escorihuela, M. J., Kerr, Y. H., de Rosnay, P., Saleh, K., Wigneron, J.-P., & Calvet, J. C. (2009). Effects of dew on the radiometric signal of a grass field at L-band. *IEEE Geoscience and Remote Sensing Letters*, *6*(1), Article 1. https://doi.org/10.1109/LGRS.2008.2000714

Farquhar, G. D., von Caemmerer, S., & Berry, J. A. (1980). A biochemical model of photosynthetic CO_2 assimilation in leaves of C_3 species. *Planta*, *149*(1), 78–90. https://doi.org/10.1007/BF00386231

Feldman, A. F., Akbar, R., & Entekhabi, D. (2018). Characterization of higher-order scattering from vegetation with SMAP measurements. *Remote Sensing of Environment*, *219*, 324–338. https://doi.org/10.1016/j.rse.2018.10.022

Feldman, A. F., Short Gianotti, D. J., Konings, A. G., Gentine, P., & Entekhabi, D. (2021). Patterns of plant rehydration and growth following pulses of soil moisture availability. *Biogeosciences*, *18*(3), 831–847. Article 3. https://doi.org/10.5194/bg-18-831-2021

Feldman, A. F., Short Gianotti, D. J., Konings, A. G., McColl, K. A., Akbar, R., Salvucci, G. D., & Entekhabi, D. (2018). Moisture pulse-reserve in the soil-plant continuum observed across biomes. *Nature Plants*, *4*(12), 1026–1033. https://doi.org/10.1038/s41477-018-0304-9

Feldman, A. F., Short Gianotti, D. J., Trigo, I. F., Salvucci, G. D., & Entekhabi, D. (2020). Land-Atmosphere drivers of landscape-scale plant water content loss. *Geophysical Research Letters*, *47*(22), e2020GL090331. https://doi.org/10.1029/2020GL090331

Ferrazzoli, P., & Guerriero, L. (1996). Passive microwave remote sensing of forests: A model investigation. *IEEE Transactions on Geoscience and Remote Sensing*, *34*(2), 433–443. Article 2. https://doi.org/10.1109/36.485121

Fink, A., Jagdhuber, T., Piles, M., Grant, J., Baur, M., Link, M., & Entekhabi, D. (2018). Estimating gravimetric moisture of vegetation using an attenuation-based multi-sensor approach. In *IGARSS 2018 - 2018 IEEE international geoscience and remote sensing symposium* (pp. 353–356). https://doi.org/10.1109/IGARSS.2018.8518949

Forkel, M., Schmidt, L., Zotta, R.-M., Dorigo, W., & Yebra, M. (2023). Estimating leaf moisture content at global scale from passive microwave satellite observations of vegetation optical depth. *Hydrology and Earth System Sciences*, *27*(1), 39–68. https://doi.org/10.5194/hess-27-39-2023

Frank, D., Reichstein, M., Bahn, M., Thonicke, K., Frank, D., Mahecha, M. D., et al. (2015). Effects of climate extremes on the terrestrial carbon cycle: Concepts, processes and potential future impacts. *Global Change Biology*, *21*(8), 2861–2880. https://doi.org/10.1111/gcb.12916

Garcia, M. N., Hu, J., Domingues, T. F., Groenendijk, P., Oliveira, R. S., & Costa, F. R. C. (2022). Local hydrological gradients structure high intraspecific variability in plant hydraulic traits in two dominant central Amazonian tree species. *Journal of Experimental Botany*, *73*(3), 939–952. https://doi.org/10.1093/jxb/erab432

Gu, L., Pallardy, S. G., Yang, B., Hosman, K. P., Mao, J., Ricciuto, D., et al. (2016). Testing a land model in ecosystem functional space via a comparison of observed and modeled ecosystem flux responses to precipitation regimes and associated stresses in a Central U.S. forest. *Journal of Geophysical Research: Biogeosciences*, *121*(7), 1884–1902. https://doi.org/10.1002/2015JG003302

Haario, H., Saksman, E., & Tamminen, J. (2001). An adaptive Metropolis algorithm. *Bernoulli*, *7*(2), Article 2. https://doi.org/10.2307/3318737

Han, X., Franssen, H.-J. H., Montzka, C., & Vereecken, H. (2014). Soil moisture and soil properties estimation in the Community Land Model with synthetic brightness temperature observations. *Water Resources Research*, *50*(7), 6081–6105. https://doi.org/10.1002/2013WR014586

Hanberry, B. B., He, H. S., & Shifley, S. R. (2016). Loss of aboveground forest biomass and landscape biomass variability in Missouri, US. *Ecological Complexity*, *25*, 11–17. https://doi.org/10.1016/j.ecocom.2015.11.001

Holtzman, N. M., Anderegg, L. D. L., Kraatz, S., Mavrovic, A., Sonnentag, O., Pappas, C., et al. (2021). L-band vegetation optical depth as an indicator of plant water potential in a temperate deciduous forest stand. *Biogeosciences*, *18*(2), 739–753. https://doi.org/10.5194/bg-18-739-2021

Hornbuckle, B. K., England, A. W., & Anderson, M. C. (2007). The effect of intercepted precipitation on the microwave emission of maize at 1.4 GHz. *IEEE Transactions on Geoscience and Remote Sensing*, *45*(7), 1988–1995. https://doi.org/10.1109/TGRS.2007.894057

Humphrey, V., & Frankenberg, C. (2023). Continuous ground monitoring of vegetation optical depth and water content with GPS signals. *Biogeosciences*, *20*(9), 1789–1811. https://doi.org/10.5194/bg-20-1789-2023

Jackson, T. J., & Schmugge, T. J. (1991). Vegetation effects on the microwave emission of soils. *Remote Sensing of Environment*, *36*(3), 203–212. https://doi.org/10.1016/0034-4257(91)90057-D

Javadian, M., Smith, W. K., Lee, K., Knowles, J. F., Scott, R. L., Fisher, J. B., et al. (2022). Canopy temperature is regulated by ecosystem structural traits and captures the ecohydrologic dynamics of a semiarid mixed conifer forest site. *Journal of Geophysical Research: Biogeosciences*, *127*(2), e2021JG006617. https://doi.org/10.1029/2021JG006617

Kachi, M., Hori, M., Maeda, T., & Imaoka, K. (2014). Status of validation of AMSR2 on board the GCOM-W1 satellite. In *2014 IEEE geoscience and remote sensing symposium* (pp. 110–113). https://doi.org/10.1109/IGARSS.2014.6946368

Katerji, N., Hallaire, M., Menoux-Boyer, Y., & Durand, B. (1986). Modelling diurnal patterns of leaf water potential in field conditions. *Ecological Modelling*, *33*(2–4), 185–203. https://doi.org/10.1016/0304-3800(86)90040-2

Kennedy, D., Swenson, S., Oleson, K. W., Lawrence, D. M., Fisher, R., Lola da Costa, A. C., & Gentine, P. (2019). Implementing plant hydraulics in the Community Land Model, Version 5. *Journal of Advances in Modeling Earth Systems*, *11*(2), 485–513. https://doi.org/10.1029/2018MS001500

Khabbazan, S., Steele-Dunne, S. C., Vermunt, P., Judge, J., Vreugdenhil, M., & Gao, G. (2022). The influence of surface canopy water on the relationship between L-band backscatter and biophysical variables in agricultural monitoring. *Remote Sensing of Environment*, *268*, 112789. https://doi.org/10.1016/j.rse.2021.112789

Khan, A. M., Stoy, P. C., Douglas, J. T., Anderson, M., Diak, G., Otkin, J. A., et al. (2021). Reviews and syntheses: Ongoing and emerging opportunities to improve environmental science using observations from the advanced baseline imager on the geostationary operational environmental satellites. *Biogeosciences*, *18*(13), 4117–4141. https://doi.org/10.5194/bg-18-4117-2021

Khatami, S., Peel, M. C., Peterson, T. J., & Western, A. W. (2019). Equifinality and flux mapping: A new approach to model evaluation and process representation under uncertainty. *Water Resources Research*, *55*(11), 8922–8941. https://doi.org/10.1029/2018WR023750

Kim, H., Parinussa, R., Konings, A. G., Wagner, W., Cosh, M. H., Lakshmi, V., et al. (2018). Global-scale assessment and combination of SMAP with ASCAT (active) and AMSR2 (passive) soil moisture products. *Remote Sensing of Environment*, *204*, 260–275. https://doi.org/10.1016/j.rse.2017.10.026

Klepper, B. (1968). Diurnal pattern of water potential in woody plants. *Plant Physiology*, *43*(12), 1931–1934. Article 12. https://doi.org/10.1104/pp.43.12.1931

Konings, A. G., & Gentine, P. (2017). Global variations in ecosystem-scale isohydricity. *Global Change Biology*, *23*(2), 891–905. Article 2. https://doi.org/10.1111/gcb.13389

Konings, A. G., Piles, M., Das, N., & Entekhabi, D. (2017). L-band vegetation optical depth and effective scattering albedo estimation from SMAP. *Remote Sensing of Environment*, *198*, 460–470. https://doi.org/10.1016/j.rse.2017.06.037

Konings, A. G., Piles, M., Rötzer, K., McColl, K. A., Chan, S. K., & Entekhabi, D. (2016). Vegetation optical depth and scattering albedo retrieval using time series of dual-polarized L-band radiometer observations. *Remote Sensing of Environment*, *172*, 178–189. https://doi.org/10.1016/j.rse.2015.11.009

Konings, A. G., Rao, K., & Steele-Dunne, S. C. (2019). Macro to micro: Microwave remote sensing of plant water content for physiology and ecology. *New Phytologist*, *223*(3), 1166–1172. https://doi.org/10.1111/nph.15808

Konings, A. G., Saatchi, S. S., Frankenberg, C., Keller, M., Leshyk, V., Anderegg, W. R. L., et al. (2021). Detecting forest response to droughts with global observations of vegetation water content. *Global Change Biology*, *27*(23), 6005–6024. https://doi.org/10.1111/gcb.15872

Kumar, S., Holmes, T. R., Bindlish, R., de Jeu, R., & Peters-Lidard, C. (2020). Assimilation of vegetation optical depth retrievals from passive microwave radiometry. *Hydrology and Earth System Sciences*, *24*(7), 3431–3450. Article 7. https://doi.org/10.5194/hess-24-3431-2020

Kumar, S., Kolassa, J., Reichle, R., Crow, W., de Lannoy, G., de Rosnay, P., et al. (2022). An agenda for land data assimilation priorities: Realizing the promise of terrestrial water, energy, and vegetation observations from space. *Journal of Advances in Modeling Earth Systems*, *14*(11), e2022MS003259. https://doi.org/10.1029/2022MS003259

Kurum, M., O'Neill, P. E., Lang, R. H., Cosh, M. H., Joseph, A. T., & Jackson, T. J. (2012). Impact of conifer forest litter on microwave emission at L-band. *IEEE Transactions on Geoscience and Remote Sensing*, *50*(4), 1071–1084. https://doi.org/10.1109/TGRS.2011.2166272

Lambers, H., Chapin, F. S., & Pons, T. L. (2008). *Plant physiological ecology* (2nd ed.). Springer.

Li, L., Yang, Z., Matheny, A. M., Zheng, H., Swenson, S. C., Lawrence, D. M., et al. (2021). Representation of plant hydraulics in the Noah-MP land surface model: Model development and multiscale evaluation. *Journal of Advances in Modeling Earth Systems*, *13*(4), e2020MS002214. https://doi.org/10.1029/2020MS002214

Li, Q., Chen, J., Moorhead, D. L., DeForest, J. L., Jensen, R., & Henderson, R. (2007). Effects of timber harvest on carbon pools in Ozark forests. *Canadian Journal of Forest Research*, *37*(11), 2337–2348. https://doi.org/10.1139/X07-086

Li, X., Wigneron, J.-P., Frappart, F., Fan, L., Ciais, P., Fensholt, R., et al. (2021). Global-scale assessment and inter-comparison of recently developed/reprocessed microwave satellite vegetation optical depth products. *Remote Sensing of Environment*, *253*, 112208. https://doi.org/10.1016/j.rse.2020.112208

Lievens, H., Al Bitar, A., Verhoest, N. E. C., Cabot, F., De Lannoy, G. J. M., Drusch, M., et al. (2015). Optimization of a radiative transfer forward operator for simulating SMOS brightness temperatures over the Upper Mississippi Basin. *Journal of Hydrometeorology*, *16*(3), 1109–1134. https://doi.org/10.1175/JHM-D-14-0052.1

Liu, Y., Holtzman, N. M., & Konings, A. G. (2021). Global ecosystem-scale plant hydraulic traits retrieved using model–data fusion. *Hydrology and Earth System Sciences*, *25*(5), 2399–2417. https://doi.org/10.5194/hess-25-2399-2021

Liu, Y., Konings, A. G., Kennedy, D., & Gentine, P. (2021). Global coordination in plant physiological and rooting strategies in response to water stress. *Global Biogeochemical Cycles*, *35*(7), Article 7. https://doi.org/10.1029/2020GB006758

Liu, Y., Parolari, A. J., Kumar, M., Huang, C.-W., Katul, G. G., & Porporato, A. (2017). Increasing atmospheric humidity and CO_2 concentration alleviate forest mortality risk. *Proceedings of the National Academy of Sciences*, *114*(37), 9918–9923. Article 37. https://doi.org/10.1073/pnas.1704811114

Liu, Y. Y., de Jeu, R. A. M., McCabe, M. F., Evans, J. P., & van Dijk, A. I. J. M. (2011). Global long-term passive microwave satellite-based retrievals of vegetation optical depth. *Geophysical Research Letters*, *38*(18), Article 18. https://doi.org/10.1029/2011GL048684

Lu, Y., Steele-Dunne, S. C., Farhadi, L., & van de Giesen, N. (2017). Mapping surface heat fluxes by assimilating SMAP soil moisture and GOES land surface temperature data. *Water Resources Research*, *53*(12), 10858–10877. https://doi.org/10.1002/2017WR021415

MacBean, N., Liddy, H., Quaife, T., Kolassa, J., & Fox, A. (2022). Building a land data assimilation community to tackle technical challenges in quantifying and reducing uncertainty in land model predictions. *Bulletin of the American Meteorological Society*, *103*(3), E733–E740. https://doi.org/10.1175/BAMS-D-21-0228.1

Martinez-Vilalta, J., Anderegg, W. R. L., Sapes, G., & Sala, A. (2019). Greater focus on water pools may improve our ability to understand and anticipate drought-induced mortality in plants. *New Phytologist*, *223*(1), 22–32. https://doi.org/10.1111/nph.15644

Matheny, A. M., Bohrer, G., Stoy, P. C., Baker, I. T., Black, A. T., Desai, A. R., et al. (2014). Characterizing the diurnal patterns of errors in the prediction of evapotranspiration by several land-surface models: An NACP analysis. *Journal of Geophysical Research: Biogeosciences*, *119*(7), 1458–1473. Article 7. https://doi.org/10.1002/2014JG002623

Matheny, A. M., Fiorella, R. P., Bohrer, G., Poulsen, C. J., Morin, T. H., Wunderlich, A., et al. (2017). Contrasting strategies of hydraulic control in two codominant temperate tree species. *Ecohydrology*, *10*(3), Article 3. https://doi.org/10.1002/eco.1815

McDowell, N., Pockman, W. T., Allen, C. D., Breshears, D. D., Cobb, N., Kolb, T., et al. (2008). Mechanisms of plant survival and mortality during drought: Why do some plants survive while others succumb to drought? *New Phytologist*, *178*(4), 719–739. https://doi.org/10.1111/j.1469-8137.2008.02436.x

Medlyn, B. E., Duursma, R. A., Eamus, D., Ellsworth, D. S., Prentice, I. C., Barton, C. V. M., et al. (2011). Reconciling the optimal and empirical approaches to modelling stomatal conductance. *Global Change Biology*, *17*(6), 2134–2144. Article 6. https://doi.org/10.1111/j.1365-2486.2010.02375.x

Mirfenderesgi, G., Matheny, A. M., & Bohrer, G. (2019). Hydrodynamic trait coordination and cost–benefit trade-offs throughout the isohydric–anisohydric continuum in trees. *Ecohydrology*, *12*(1), e2041. https://doi.org/10.1002/eco.2041

Mironov, V. L., Dobson, M. C., Kaupp, V. H., Komarov, S. A., & Kleshchenko, V. N. (2002). Generalized refractive mixing dielectric model for moist soils. In *IEEE international geoscience and remote sensing symposium* (Vol. 6, pp. 3556–3558). https://doi.org/10.1109/IGARSS.2002.1027247

Mo, T., Choudhury, B. J., Schmugge, T. J., Wang, J. R., & Jackson, T. J. (1982). A model for microwave emission from vegetation-covered fields. *Journal of Geophysical Research*, *87*(C13), 11229–11237. https://doi.org/10.1029/JC087iC13p11229

Momen, M., Wood, J. D., Novick, K. A., Pangle, R., Pockman, W. T., McDowell, N. G., & Konings, A. G. (2017). Interacting effects of leaf water potential and biomass on vegetation optical depth: Effects of LWP and biomass on VOD. *Journal of Geophysical Research: Biogeosciences*, *122*(11), 3031–3046. https://doi.org/10.1002/2017JG004145

Munger, W., & Wofsy, S. (2020). Biomass inventories at Harvard forest EMS Tower since 1993 [Dataset]. Environmental Data Initiative. https://doi.org/10.6073/PASTA/C27CDE917CCC89CA0A131525FCD328B8

Myneni, R. B., Hoffman, S., Knyazikhin, Y., Privette, J. L., Glassy, J., Tian, Y., et al. (2002). Global products of vegetation leaf area and fraction absorbed PAR from year one of MODIS data. *Remote Sensing of Environment*, *83*(1–2), 214–231. Article 1–2. https://doi.org/10.1016/S0034-4257(02)00074-3

Nelson, J. A., Carvalhais, N., Migliavacca, M., Reichstein, M., & Jung, M. (2018). Water-stress-induced breakdown of carbon–water relations: Indicators from diurnal FLUXNET patterns. *Biogeosciences*, *15*(8), 2433–2447. https://doi.org/10.5194/bg-15-2433-2018

Nolan, R. H., Boer, M. M., Resco de Dios, V., Caccamo, G., & Bradstock, R. A. (2016). Large-scale, dynamic transformations in fuel moisture drive wildfire activity across southeastern Australia: Transformations in Fuel Moisture. *Geophysical Research Letters*, *43*(9), Article 9. https://doi.org/10.1002/2016GL068614

Norton, A. J., Rayner, P. J., Koffi, E. N., Scholze, M., Silver, J. D., & Wang, Y.-P. (2019). Estimating global gross primary productivity using chlorophyll fluorescence and a data assimilation system with the BETHY-SCOPE model. *Biogeosciences*, *16*(15), 3069–3093. https://doi.org/10.5194/bg-16-3069-2019

Novick, K. A., Ficklin, D. L., Baldocchi, D., Davis, K. J., Ghezzehei, T. A., Konings, A. G., et al. (2022). Confronting the water potential information gap. *Nature Geoscience*, *15*(3), 158–164. https://doi.org/10.1038/s41561-022-00909-2

O'Neill, P. E., Bindlish, R., Chan, S., Chaubell, J., Njoku, E. G., & Jackson, T. J. (2019). *SMAP algorithm theoretical basis document: Level 2 & 3 soil moisture (passive) data products*. Jet Propulsion Laboratory.

Pallardy, S. G., Gu, L., Wood, J. D., Hosman, K. P., & Sun, Y. (2018). Predawn leaf water potential of oak-hickory forest at Missouri Ozark (MOFLUX) Site: 2004-2020 [Dataset]. ORNLTESSFA (Oak Ridge National Lab's Terrestrial Ecosystem Science Scientific Focus Area (ORNL TES SFA)). https://doi.org/10.3334/CDIAC/ORNLSFA.004

Proß, T., Bruelheide, H., Potvin, C., Sporbert, M., Trogisch, S., & Haider, S. (2021). Drivers of within-tree leaf trait variation in a tropical planted forest varying in tree species richness. *Basic and Applied Ecology*, *50*, 203–216. https://doi.org/10.1016/j.baae.2020.11.001

Rao, K., Anderegg, W. R. L., Sala, A., Martínez-Vilalta, J., & Konings, A. G. (2019). Satellite-based vegetation optical depth as an indicator of drought-driven tree mortality. *Remote Sensing of Environment*, *227*, 125–136. https://doi.org/10.1016/j.rse.2019.03.026

Rao, K., Williams, A. P., Diffenbaugh, N. S., Yebra, M., & Konings, A. G. (2022). Plant-water sensitivity regulates wildfire vulnerability. *Nature Ecology & Evolution*, *6*(3), 332–339. https://doi.org/10.1038/s41559-021-01654-2

Reichle, R. H., De Lannoy, G. J. M., Liu, Q., Ardizzone, J. V., Colliander, A., Conaty, A., et al. (2017). Assessment of the SMAP Level-4 surface and root-zone soil moisture product using in situ measurements. *Journal of Hydrometeorology*, *18*(10), 2621–2645. https://doi.org/10.1175/JHM-D-17-0063.1

Renner, M., Brenner, C., Mallick, K., Wizemann, H.-D., Conte, L., Trebs, I., et al. (2019). Using phase lags to evaluate model biases in simulating the diurnal cycle of evapotranspiration: A case study in Luxembourg. *Hydrology and Earth System Sciences*, *23*(1), 515–535. https://doi.org/10.5194/hess-23-515-2019

Reyer, C. P. O., Leuzinger, S., Rammig, A., Wolf, A., Bartholomeus, R. P., Bonfante, A., et al. (2013). A plant's perspective of extremes: Terrestrial plant responses to changing climatic variability. *Global Change Biology*, *19*(1), 75–89. https://doi.org/10.1111/gcb.12023

Shan, X., Steele-Dunne, S., Huber, M., Hahn, S., Wagner, W., Bonan, B., et al. (2022). Towards constraining soil and vegetation dynamics in land surface models: Modeling ASCAT backscatter incidence-angle dependence with a Deep Neural Network. *Remote Sensing of Environment*, *279*, 113116. https://doi.org/10.1016/j.rse.2022.113116

Silva, M., Matheny, A. M., Pauwels, V. R. N., Triadis, D., Missik, J. E., Bohrer, G., & Daly, E. (2022). Tree hydrodynamic modelling of the soil–plant–atmosphere continuum using FETCH3. *Geoscientific Model Development*, *15*(6), 2619–2634. https://doi.org/10.5194/gmd-15-2619-2022

Skelton, R. P., West, A. G., & Dawson, T. E. (2015). Predicting plant vulnerability to drought in biodiverse regions using functional traits. *Proceedings of the National Academy of Sciences*, *112*(18), 5744–5749. https://doi.org/10.1073/pnas.1503376112

Steele-Dunne, S. C., Friesen, J., & van de Giesen, N. (2012). Using diurnal variation in backscatter to detect vegetation water stress. *IEEE Transactions on Geoscience and Remote Sensing*, *50*(7), 2618–2629. https://doi.org/10.1109/TGRS.2012.2194156

Still, C. J., Page, G., Rastogi, B., Griffith, D. M., Aubrecht, D. M., Kim, Y., et al. (2022). No evidence of canopy-scale leaf thermoregulation to cool leaves below air temperature across a range of forest ecosystems. *Proceedings of the National Academy of Sciences*, *119*(38), e2205682119. https://doi.org/10.1073/pnas.2205682119

Sun, D., & Pinker, R. (2003). Estimation of land surface temperature from a Geostationary Operational Environmental Satellite (GOES-8). *Journal of Geophysical Research*, *108*(D11), 4326. https://doi.org/10.1029/2002JD002422

Tang, J., & Zhuang, Q. (2008). Equifinality in parameterization of process-based biogeochemistry models: A significant uncertainty source to the estimation of regional carbon dynamics: Equifinality in regional carbon dynamics. *Journal of Geophysical Research*, *113*, G04010. https://doi.org/10.1029/2008JG000757

Tindall, J. A., Kunkel, J. R., & Anderson, D. E. (1999). *Unsaturated zone hydrology for scientists and engineers*. Prentice Hall.

Turner, N. C. (1988). Measurement of plant water status by the pressure chamber technique. *Irrigation Science*, *9*(4), 289–308. https://doi.org/10.1007/BF00296704

Ulaby, F. T., & Long, D. G. (2014). *Microwave radar and radiometric remote sensing*. The University of Michigan Press.

van Genuchten, M. (1980). A closed-form equation for predicting the hydraulic conductivity of unsaturated soils. *Soil Science Society of America Journal*.

Vereecken, H., Amelung, W., Bauke, S. L., Bogena, H., Brüggemann, N., Montzka, C., et al. (2022). Soil hydrology in the Earth system. *Nature Reviews Earth & Environment*, *3*(9), 573–587. https://doi.org/10.1038/s43017-022-00324-6

Wang, H., Wigneron, J.-P., Ciais, P., Yao, Y., Fan, L., Liu, X., et al. (2023). Seasonal variations in vegetation water content retrieved from microwave remote sensing over Amazon intact forests. *Remote Sensing of Environment*, *285*, 113409. https://doi.org/10.1016/j.rse.2022.113409

Wang, Y., Braghiere, R. K., Longo, M., Norton, A. J., Köhler, P., Doughty, R., et al. (2023). Modeling global vegetation gross primary productivity, transpiration and hyperspectral canopy radiative transfer simultaneously using a next generation land surface model—CliMA Land. *Journal of Advances in Modeling Earth Systems*, *15*(3), e2021MS002964. https://doi.org/10.1029/2021MS002964

Wang, Y., Köhler, P., He, L., Doughty, R., Braghiere, R. K., Wood, J. D., & Frankenberg, C. (2021). Testing stomatal models at the stand level in deciduous angiosperm and evergreen gymnosperm forests using CliMA Land (v0.1). *Geoscientific Model Development*, *14*(11), 6741–6763. https://doi.org/10.5194/gmd-14-6741-2021

Wigneron, J.-P., Jackson, T. J., O'Neill, P., De Lannoy, G., de Rosnay, P., Walker, J. P., et al. (2017). Modelling the passive microwave signature from land surfaces: A review of recent results and application to the L-band SMOS & SMAP soil moisture retrieval algorithms. *Remote Sensing of Environment*, *192*, 238–262. https://doi.org/10.1016/j.rse.2017.01.024

Wood, J. D., & Gu, L. (2022). AmeriFlux FLUXNET-1F US-MOz Missouri Ozark Site [Dataset]. AmeriFlux; Oak Ridge National Laboratory; University of Missouri. https://doi.org/10.17190/AMF/1854370

Wood, J. D., Gu, L., Hanson, P., Frankenberg, C., & Sack, L. (2022). Supporting biophysical data for "The ecosystem wilting point defines drought response and recovery of a Quercus-Carya forest" [Dataset]. Zenodo. https://doi.org/10.5281/ZENODO.7477878

Wood, J. D., Gu, L., Hanson, P. J., Frankenberg, C., & Sack, L. (2023). The ecosystem wilting point defines drought response and recovery of a *Quercus-Carya* forest. *Global Change Biology*, *29*(7), 2015–2029. https://doi.org/10.1111/gcb.16582

Wu, G., Guan, K., Li, Y., Novick, K. A., Feng, X., McDowell, N. G., et al. (2021). Interannual variability of ecosystem iso/anisohydry is regulated by environmental dryness. *New Phytologist*, *229*(5), 2562–2575. https://doi.org/10.1111/nph.17040

Xiao, J., Fisher, J. B., Hashimoto, H., Ichii, K., & Parazoo, N. C. (2021). Emerging satellite observations for diurnal cycling of ecosystem processes. *Nature Plants*, *7*(7), 877–887. https://doi.org/10.1038/s41477-021-00952-8

Xu, S., McVicar, T. R., Li, L., Yu, Z., Jiang, P., Zhang, Y., et al. (2022). Globally assessing the hysteresis between sub-diurnal actual evaporation and vapor pressure deficit at the ecosystem scale: Patterns and mechanisms. *Agricultural and Forest Meteorology*, *323*, 109085. https://doi.org/10.1016/j.agrformet.2022.109085

Xu, T., Bateni, S. M., Neale, C. M. U., Auligne, T., & Liu, S. (2018). Estimation of turbulent heat fluxes by assimilation of land surface temperature observations from GOES satellites into an ensemble Kalman smoother framework. *Journal of Geophysical Research: Atmospheres*, *123*(5), 2409–2423. https://doi.org/10.1002/2017JD027732

Xu, X., Konings, A. G., Longo, M., Feldman, A., Xu, L., Saatchi, S., et al. (2021). Leaf surface water, not plant water stress, drives diurnal variation in tropical forest canopy water content. *New Phytologist, nph*, *231*(1), 122–136. https://doi.org/10.1111/nph.17254

Yebra, M., Dennison, P. E., Chuvieco, E., Riaño, D., Zylstra, P., Hunt, E. R., et al. (2013). A global review of remote sensing of live fuel moisture content for fire danger assessment: Moving towards operational products. *Remote Sensing of Environment*, *136*, 455–468. https://doi.org/10.1016/j.rse.2013.05.029

Young, F. J., Radatz, C. A., & Marshall, C. A. (2001). *Soil survey of Boone County, Missouri*. USDA NRCS.

Yu, Y., Tarpley, D., Privette, J. L., Flynn, L. E., Xu, H., Chen, M., et al. (2012). Validation of GOES-R satellite land surface temperature algorithm using SURFRAD ground measurements and statistical estimates of error properties. *IEEE Transactions on Geoscience and Remote Sensing*, *50*(3), 704–713. https://doi.org/10.1109/TGRS.2011.2162338

Yu, Z., Wang, J., Liu, S., Rentch, J. S., Sun, P., & Lu, C. (2017). Global gross primary productivity and water use efficiency changes under drought stress. *Environmental Research Letters*, *12*(1), 014016. https://doi.org/10.1088/1748-9326/aa5258

Zeng, X., Atlas, R., Birk, R. J., Carr, F. H., Carrier, M. J., Cucurull, L., et al. (2020). Use of observing system simulation experiments in the United States. *Bulletin of the American Meteorological Society*, *101*(8), E1427–E1438. https://doi.org/10.1175/BAMS-D-19-0155.1

Zhang, Q., Manzoni, S., Katul, G., Porporato, A., & Yang, D. (2014). The hysteretic evapotranspiration-Vapor pressure deficit relation: ET-VPD hysteresis. *Journal of Geophysical Research: Biogeosciences*, *119*(2), Article 2. https://doi.org/10.1002/2013JG002484

References From the Supporting Information

Gelman, A., & Rubin, D. B. (1992). Inference from iterative simulation using multiple sequences. *Statistical Science*, *7*(4), 457–472. https://doi.org/10.1214/ss/1177011136

Klein, T. (2014). The variability of stomatal sensitivity to leaf water potential across tree species indicates a continuum between isohydric and anisohydric behaviours. *Functional Ecology*, *28*(6), 1313–1320. https://doi.org/10.1111/1365-2435.12289

Liu, Y., Kumar, M., Katul, G. G., Feng, X., & Konings, A. G. (2020). Plant hydraulics accentuates the effect of atmospheric moisture stress on transpiration. *Nature Climate Change*, *10*(7), 691–695. Article 7. https://doi.org/10.1038/s41558-020-0781-5

Manzoni, S., Katul, G., & Porporato, A. (2014). A dynamical system perspective on plant hydraulic failure. *Water Resources Research*, *50*(6), 5170–5183. https://doi.org/10.1002/2013WR015236

Martin-StPaul, N., Delzon, S., & Cochard, H. (2017). Plant resistance to drought depends on timely stomatal closure. *Ecology Letters*, *20*(11), 1437–1447. https://doi.org/10.1111/ele.12851